Complex susceptibility and pinning potential in low anisotropic superconductors

Thesis Submitted for the Degree of

Doctor of Philosophy (Science) in Physics

by

Shoumi Roy

of

Jadavpur University

under the supervision of

Professor Ajay Kumar Ghosh

Department of Physics

Jadavpur University

Kolkata 700032, India

যাদবপুর বিশ্ববিদ্যালয়
কলকাতা - ৭০০০৩২, ভারত

*JADAVPUR UNIVERSITY
KOLKATA - 700032, INDIA

FACULTY OF SCIENCE: DEPARTMENT OF PHYSICS

Certificate from the Supervisor

This is to certify that the thesis entitled "**Complex susceptibility and pinning potential in low anisotropic superconductors**" submitted by **Shoumi Roy**, who got her name registered on **23.04.2015 (Index No: 39/15/Phys/23)** for the award of Ph.D. (Science) degree of Jadavpur University, is absolutely based upon her work under the supervision of **Prof. Ajay Kumar Ghosh** and that neither this thesis nor any part of it has been submitted for either any degree/diploma or any other academic award anywhere before.

Professor Dr. Ajay Kumar Ghosh
Department of Physics
Jadavpur University
Kolkata-700032

Ajay Kumar Ghosh 08/09/2022

(Prof. Ajay Kumar Ghosh)
Signature of Supervisor
with Date and Official Seal

*Established on and from 24th December, 1955 vide Notification No. 10986-Edn/IU-42/55 dated 6th December, 1955 under Jadavpur University Act, 1955 (West Bengal Act XXXIII of 1955) followed by Jadavpur University Act, 1981 (West Bengal Act XXIV of 1981)

ফোন: ০৩৩-২৪১৪-৬৬৬৬ Ext. ২৭৬১
মো: +৯১-৯৮৩০৮৪৮৯২০

Website: www.jaduniv.edu.in

Phone: 033-2414-6666 Ext. 2761
M: +91-9830848920
Email: ajayk.ghosh@jadavpuruniversity.in

Acknowledgments

I would like to express my sincere gratitude and regards towards my supervisor, Prof. Ajay Kumar Ghosh, Department of Physics, Jadavpur University, for the opportunity to conduct research on the topic, "Complex susceptibility and pinning potential in low anisotropic superconductors". I would like to respectfully acknowledge his support and guidance in conducting this research project and in writing this thesis.

I would like to thank all my colleagues and fellow PhD scholars from the AKG group at Jadavpur University.

I would like to thank the Department of Science and Technology, Government of West Bengal, for their State Fellowship which funded this thesis.

I would like to thank my parents, siblings and friends for their support.

Contents

List of Publications and Conferences

Articles in Journals

1. **S. Roy**, Ajay Kumar Ghosh, Physica C 580 (2021) 1353766.

2. **S. Roy**, Ajay Kumar Ghosh, "Dynamics of local magnetic field profile in disordered superconductors", 2021, submitted.

3. **S. Roy**, Ajay Kumar Ghosh, "Complex susceptibility in Repetitive Gaussian and Rademacher pinned 2D samples with low anisotropy", 2021, in preparation.

Poster Presentation in National and International Conferences:

1. **Roy, S.**, Ghosh, A.K., "Magnetic field profile in two dimensional superconducting networks below the critical temperature", Third International Conference on Advanced Materials (ICAM 2019), Kottayam, Kerala, India, 9-11

August 2019.

2. **Roy, S.**, Ghosh, A.K., "Impact of repetitive Gaussian pinning force density on some specific distribution of superconducting grains", International Conference on Complex and Functional Materials (ICCFM 2018), Kolkata, West Bengal, India, 13-16 December 2018.

3. **Roy, S.**, Ghosh, A.K., "Pinning dependence of internal field profile in model superconducting networks", National Conference on Recent Trends in Condensed Matter Physics, Kolkata, West Bengal, India, 31 October -3 November 2017.

4. **Roy, S.**, Ghosh, A.K., "Numerical studies on field profile in disordered pnictide superconductor", 25th National Conference on Condensed Matter Physics "Condensed Matter Days – 2017" (CMDAYS17), Tezpur University, Tezpur, Assam, India, 29-31 August 2017.

Poster Presentation in Departmental Conference:

1. **Roy, S.**, Ghosh, A.K., "Numerical studies on internal field profile and complex susceptibility", Recent Trends in Frontier research in Physics, 6 March 2018.

2. **Roy, S.**, Ghosh, A.K., "Time dependence of microscopic field profile in

pnictide", Twists and Turns in Physics Research: Special Emphasis on Condensed Matter and Biophysics (TTPR -2017), 21-22 February 2017.

3. **Roy, S.**, Ghosh, A.K., "On the critical state model and internal magnetic field distribution in a pnictide superconductor", Some Recent Trends in Research in Physics (SRTRP – 2016), 21 March 2016.

Chapter 1

Background and Objectives

1.1 Introduction

Type II superconductors, when subjected to magnetic fields above a certain threshold, show a variety of magnetic properties due to penetration of quantized flux inside the superconductors. Field penetration depends on the internal properties of the superconducting sample like position and distribution of grain clusters, and external properties like the shape and size of the sample as well as the nature of the incident magnetic field. Critical current in such samples, is a function of the internal magnetic field and can be inversely or exponentially dependent on incident magnetic field. Critical field can also be independent of incident magnetic field. As it is the maximum loss less current inside the superconducting sample, numerous numerical studies have been undertaken to map the exact dependence of critical current on sample geometry and local field inside the sample, in an attempt to maximize critical current. Critical state equation has also been used to

estimate the nature of local field profile inside the sample. Global magnetic properties of superconductors like complex susceptibility can be obtained from critical state equation.

1.2 Review

Starting from a critical current whose magnitude is independent of magnitude of local magnetic field and depends on only the presence of magnetic field inside the sample, Bean (1) obtained analytic expressions for local field profile inside superconducting samples. Incident magnetic field is assumed to be perpendicular to the sample and the negative or positive value of critical current is determined by change in local magnetic field compared to earlier times. Field penetration is only important along one sample dimension.

Apart from this field independent critical current model, critical current with exponential field dependence or inverse field dependence (2) have also been used to solve for magnetic properties in samples with infinite height and equal length and breadth (8). Various other ratios of length to breadth are also considered and field penetration obtained in such cases. A generalized critical current is also developed by Xu et al (11) which gives the following relation between critical

current density and local field:

$$J_c(H_i,T) = J_c(T)/\left[1+H_i/H_0(T)\right]^{\beta} \tag{1.1}$$

where β is a dimensionless constant.

In recent years, samples of arbitrary shapes placed in magnetic field with in plane non-zero component have also been modelled by using critical state equations (5; 10) , where flux is not pinned but flux cutting doesn't occur.

1.3 Objective

Depending on the pinning landscape in superconducting systems the enhancement in the critical current density is possible. Even though in experimental studies it is extremely difficult to have an exact idea about the pinning landscape, in numerical studies it is not impossible. Following different theories attempts have been made to obtain the way of attaining maximum critical current. However, it is very important to understand how local pinning force density affects critical current density. Internal field profile in presence of any particular pinning landscape governs local current density which is very essential to overall enhancement. Complex susceptibility and pinning potential are known to be strongly related via the local field profile. In the present work we have addressed different aspects of the aforementioned ideas in low anisotropic superconducting systems in which

pinning potentials are known to be very strong. Critical state model is known to be very successful in finding the local field profile in a superconducting system (2). We have proposed that the pinning force density depends not only on temperature but also on the position coordinate. We have modified and followed the finite temperature critical state model to calculate the complex susceptibility as a function of temperature. We have considered low anisotropic superconducting systems within the framework of the critical state model.

In Mueller's model the proportionality constant in the $j_c \propto \frac{1}{H}$ relation is given as the pinning force density. Pinning force density is considered to be a function of temperature and on the position where the local field is calculated is situated, in grains or in the weak links between grains. We considered different grain size distributions and found field profile inside the sample to be independent of the grain size distribution for same average grain radius. This being the case, we have modelled uniform grain size with uniform gap between grains.

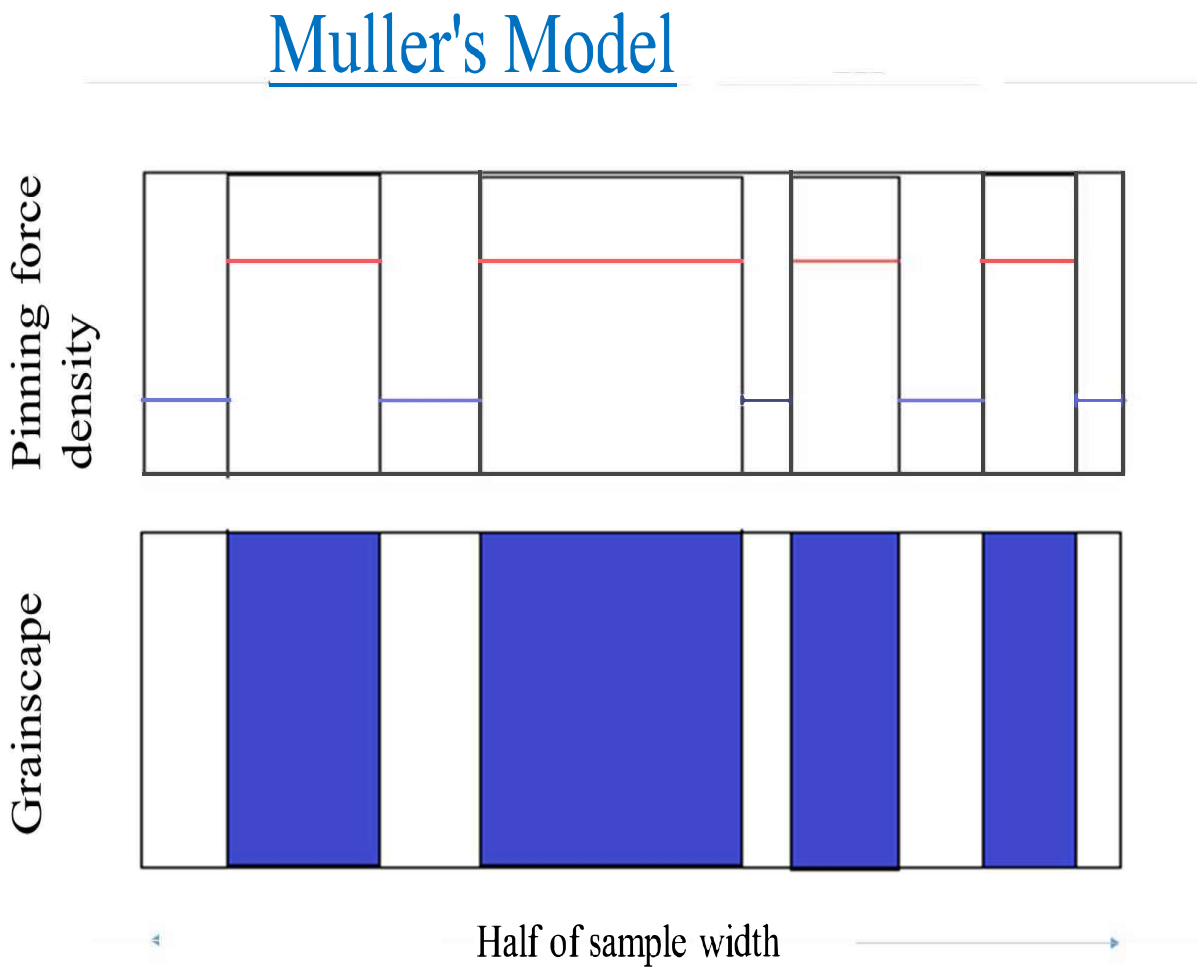

Figure 1.1: Schematic of Mueller's Model

In the first model, we considered granular superconductors with uniform distribution of grains throughout the sample. The grain boundaries form the weak links with pinning force densities much less than that in the superconducting grains. Penetration depth was assumed to have a power law temperature dependence, with the exponent taken as 2. Pinning force density is treated as function of temperature and field. Increase in penetration depth with temperature and decrease in pinning force density with temperature compete to influence the local field inside weak links and grains. Susceptibility is computed by averaging local magnetic field over time period of external field profile and the finite sample dimension. We change the amplitude of the ac (cosine) magnetic field while keeping the dc magnetic field constant and study the system. Later, we use ac magnetic field. Next, we consider a scenario where the pinning force density is a function of field itself. Starting from Mueller's model where pinning force density is independent of field (2), we increment the exponent slowly till pinning force density is directly proportional to field and study its effects on field penetration and field profile. In the next model we considered granular superconductors with non-uniform distribution of grains in the sample. The sample is separated into grains clusters made of grains with weak link boundaries and grain free separations, with the grain clusters and separations equal in length. Pinning force density is assumed to be a function of temperature and position inside the sample. Pinning force density inside the grain is much higher than the other two regions and con-

stant throughout the grain. In the first sample programmed, pinning force density in the separations and weak links has the functional form of repetitive truncated Gaussians with peaks lying at the centers of the separations and truncations either at the edge of the sample or in the midpoints of the grain clusters. In the second sample programmed, pinning force density in all the separations is assumed to be constant and in the weak links between grains in the grain clusters, it is assumed to be zero. Susceptibility across the entire temperature range is calculated. The effect of varying the maximum value of pinning force density on T_p in either scenario is also studied.

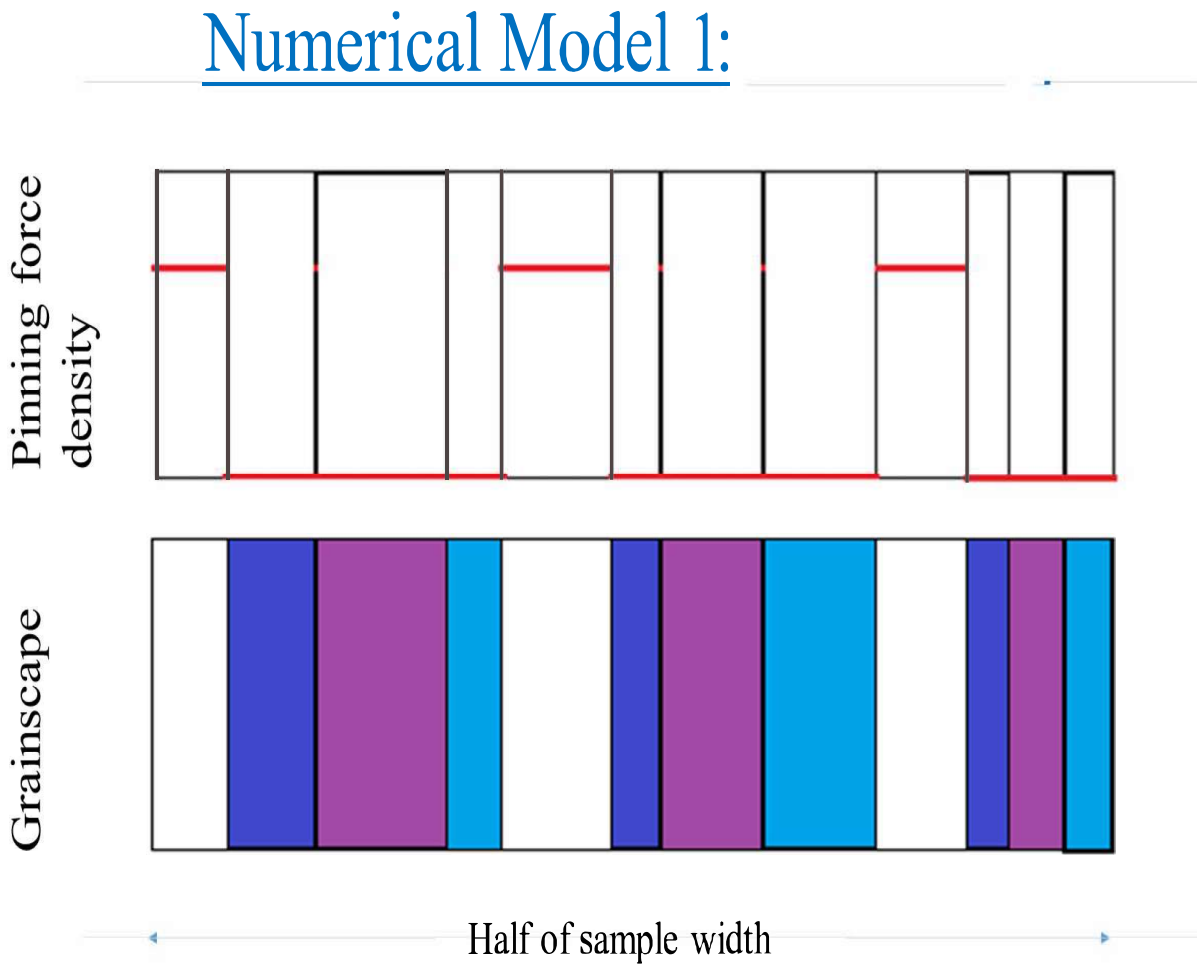

Figure 1.2: Schematic of model where pinning force density minima coincides with grain clusters, developed first to study granular superconductors

1.4 Numerical Model

Final model under consideration is disordered granular superconductor with grain clusters and grain-free separations. Presence of disorder increases the pinning force density in the separations. The pinning force density in the grain is, in this model, much lower than the pinning force density in the separations. There are no weak links in the grain clusters. Pinning force density has the same functional form in the grain clusters and the separations, including the same temperature dependence and same functional dependence on position. In the first scenario, pinning force density in the separations and grain clusters has the functional form of repetitive truncated Gaussians with peaks lying at the centers of the separations and truncations either at the edge of the sample or in the midpoints of the grain clusters. In the second scenario, pinning force density in all the separations is assumed to be constant and in the grain clusters, it is assumed to be zero. In such grainscaped sample, we have solved the critical state equation separately for the grained and grain-free segments, taking into account the effective permeability of the region in question. Quadratic temperature dependence of penetration depth is assumed as pnictides are the main group of samples we have modelled and quadratic temperature dependence is experimentally observed in pnictides.

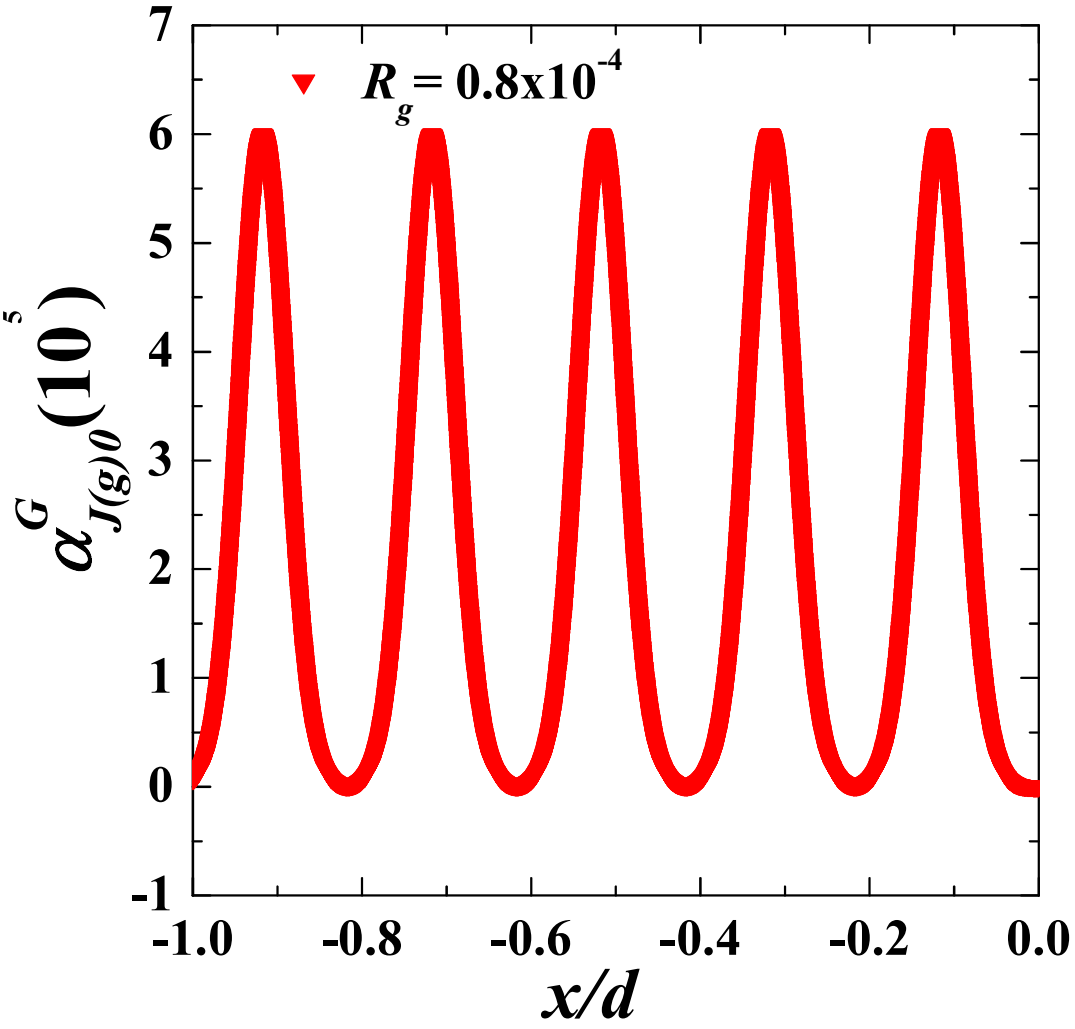

Figure 1.3: Schematic of Gaussian pinning in final model developed to study granular superconductors. Same Gaussian functional form is used for both the grain clusters and the grain free regions.

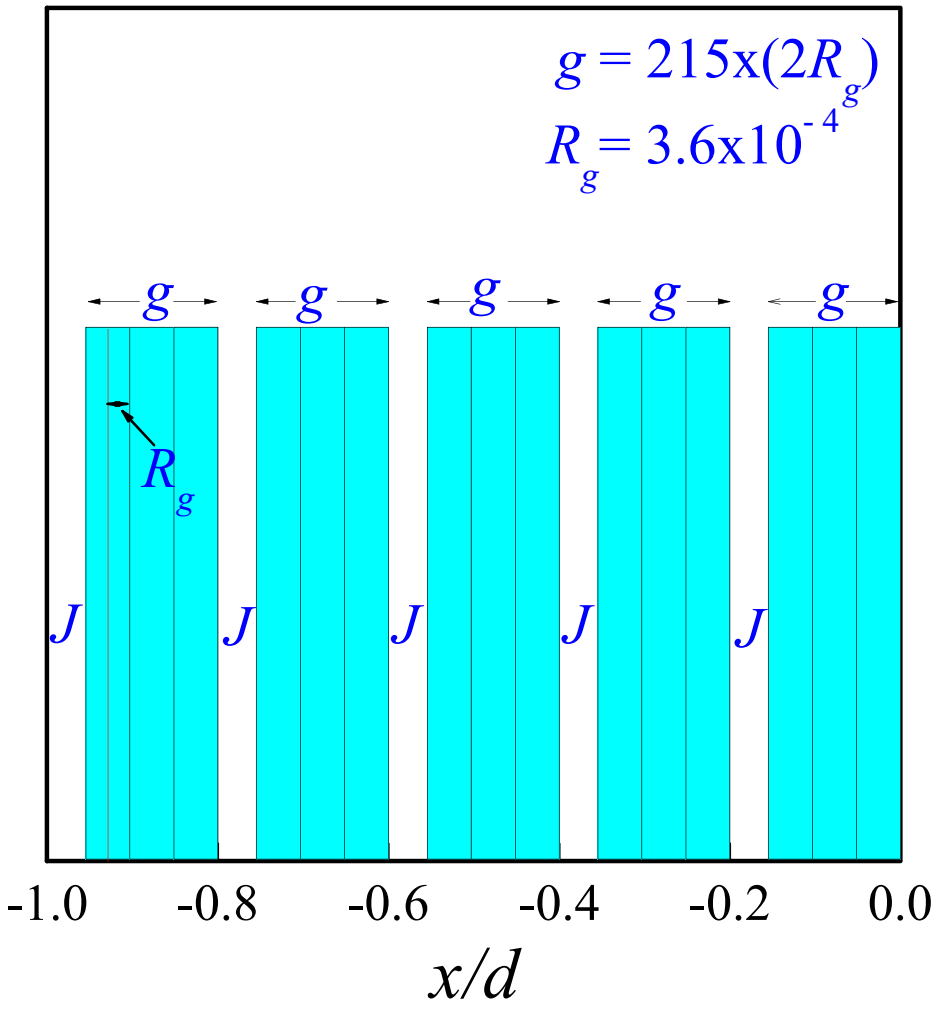

Figure 1.4: Schematic of grain distribution in granular superconductor

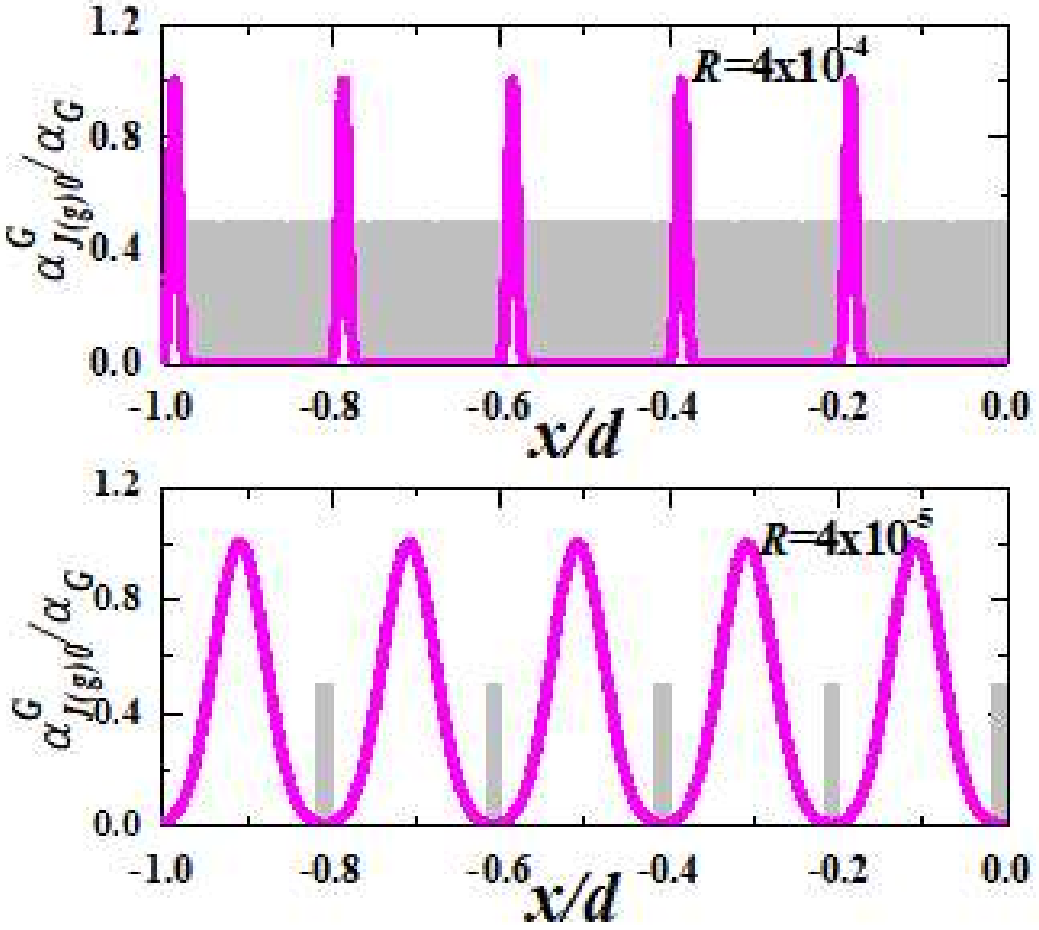

Figure 1.5: Schematic of two Repetitive Gaussian pinned granular sample with grain clusters (grey) and Repetitive Gaussian spatial pinning profile

We have simplified the model by considering grains of identical dimensions in any given superconducting sample. We have verified that assuming normal or triangular distribution of grain size along the same average grain radius, does not change the field penetration.

1.5 Thesis outline

The subject matter of the thesis is presented in the following five chapters,

1. Chapter-1 Background and Objectives of the project are explained in detail here. Review of existing literature is provided. Various numerical models in existing literature are discussed. Mueller's model is explained in detail. Various models that we have developed are also discussed alongside diagrams detailing form of pinning density profiles. Different relative positions of pinning profile maxima and grain clusters, and different dependences of critical current density on local field profile and superconducting fractions are highlighted.

2. Chapter-2 The penetration of the magnetic field in a network consisting of the superconducting grains and intergranular region depends not only on the applied external magnetic field but also on the underlying pinning force density and fraction of the superconducting grains in the sample. Considering

the underlying pinning force density in the form of the repetitive Gaussian (RG) nature we have solved the critical state model to get the spatial internal field profile at a particular time instant. The internal magnetic field as a function of the position inside the superconductor exhibits nonlinear, step-like nature. The complicated nature of the penetration of the field gets strongly affected by the size of the granular region and the total pinning force density in the superconductors. We have numerically calculated the real and imaginary parts of the complex susceptibility. The variation of the imaginary part with the temperature has a peak at a temperature which shifts towards the higher temperature with the reduction of the superconducting fraction.

3. Chapter 3 We solve the critical state equation with pinning force density separable into functions of temperature and position numerically to find the distribution of the internal magnetic field using a form of the London penetration depth suitable for pnictide superconductors. Rademacher function and repetitive Gaussian forms of the pinning force density have been modelled. Superconducting grains are assumed to be embedded within two normal regions in Josephson junctions. Pinning force density is considered to be higher in the normal regions as compared to that of the regions with grains by several orders of magnitude. Over a wide range of temperature below the critical temperature we have calculated and analysed local field profile at a particular time instant using an external ac magnetic field. Time variation of

the local field at several positions has been calculated for both types of the variation of the pinning force density.

4. Chapter-4 We extend the 1D model to two dimensions assuming symmetry along both x and y directions perpendicular to the incident magnetic field. We program both types of pinning density profiles and multiple values of grain radii and pinning magnitudes. We then compare the results with the 1D case to identify similarities and differences between the 1D and 2D sample models and try to identify causes behind any such changes.

5. Appendix I The C code used to model the Repetitive Gaussian pinned sample is provided in its entirety in Appendix I.

6. Appendix II Changes in the code for the 2D sample are mentioned in the Appendix II.

References

[1] C. P. Bean, Rev. Mod. Phys. **36** (1964) 31

[2] K. H. Muller, Physica C **159** (1989) 717

[3] J. R. Clem, J. Appl. Phys.50 (1979) 3518

[4] J. R. Clem, A. Sanchez, Phys. Rev. **B 50** (1994) 9355

[5] E. H. Brandt, G. P. Mikitik, Phys. Rev. **B76** (2007) 064526

[6] I. M. Babich, G. P. Mikitik, E. H. Brandt, Phys. Rev. **B 74** (2006) 224501

[7] E. H. Brandt and M. Indenbom, Phys. Rev. B **48**, 12893(1993)

[8] D.-X. Chen, A. Sanchez, J. Nogues, J. S. Muoz, Phys. Rev. **B 41** (1990) 9510

[9] D.-X. Chen, E. Pardo, A. Sanchez, S.-S. Wang, Z.-H. Han, E. Bartolome, T. Puig, X. Obradors, Phys. Rev. **B 72** (2005) 052504

[10] G. P. Mikitik, J. Low temp. Phys. **36** (2010) 13

[11] M. Xu, D. Shi, R. F. Fox, Phys. Rev. **B 42** (1990) 10773

[12] L. Ji, R. H. Sohn, G. C. Spalding, C. J. Lobb, M. Tinkham, Phys. Rev. **B 40** (1989) 10936

[13] K. H. Muller, S. K. H. Lam, X. L. Wang, S. X. Dou, Phys. Rev. **B 85** (2012) 224516

[14] K.-H. Muller, M. Nikolo, R. Driver, Phys. Rev. **B 43** (1991) 7976

[15] G. Blatter, M. V. Feigelman, V. B. Geshkenbein, A. I. Larkin, V. M. Vinokur, Rev. Mod. Phys. **66** (1994) 1125

[16] M. J. Qin, X. X. Yao, Phys. Rev. **B54** (1996) 7536

[17] F. Gomory, P. Lobotka, Solid State Comm. **66** (1988) 645

[18] M. G. das Virgens, S. García, M. A. Continentino, L. Ghivelder, Phys. Rev. **B 71** (2005) 064520

[19] J.Z. Sun, M. J.Scharen, L. C. Bourne, and J.R. Schrieffer, Phys. Rev. **B44** (1991) 5275

[20] R. B. Flippen, Phys. Rev. **B45** (1992) 12498

[21] T. H. Johansen and H. Bratsberg, J. Appl. Phys. **77**, 3945(1995)

[22] D. Dew-Hughes, Phil. Mag. 30 (1974) 293.

[23] C.Romero-Salazar and F.Pérez-Rodŕiguez, Appl. Phys. Lett. **83**, 5256(2003)

[24] H. Dersch and G. Blatter, Phys. Rev. B **38**, 11391 (1988)

[25] M. Däumling and D. C. Larbalestier, Phys. Rev. B **40**, 9350(R)(1989)

[26] L. W. Conner and A. P. Malozemoff, Phys. Rev. B **43**, 402(1991)

Chapter 2

Pinning mediated field penetration and complex susceptibility in inhomogeneous superconductors

2.1 Introduction

The determination of the internal field profile inside a superconductor is always very challenging both experimentally and numerically. It can have an exponential, linear and other nature depending on several internal and external factors (1; 2; 3; 4). The penetration of the magnetic field in a superconducting network is very complex in nature in presence of a particular underlying pinning force density. An internal distribution of the local magnetic field is governed by several internal factors (5). The competition in the roles of the spatial distribution of the pinning force density and size of the grain in controlling the internal field profile remains very unclear. Any deliberately introduced defects in the sample will change pinning force density of the sample and hence the diamagnetic response

of the superconductor. There are several studies in superconducting systems in which local field profile has been calculated in different ways (6; 7; 8). The critical state model is very efficient to study the internal field profile numerically (9). In (9) Muller, introduces various assumptions like $H_{c1} = 0$ and introduction of constants H_{J0} and H_{g0} in critical state equations for non-granular regions and for granular clusters respectively, for finite current density when local field profile is zero. Surface effects due to sample boundaries is ignored. For an external ac magnetic field the internal field profile is related to the complex susceptibility. The variation of the real and imaginary parts of the ac susceptibility with temperature in superconducting systems is commonly used to understand flux pinning properties (10; 11).

In this letter we have modelled the pinning force density by repeating a particular functional form and named it as the repetitive Gaussian (RG) form. Such a modelling presupposes that defects in the superconductor can be deliberately changed to give rise to a RG form of pinning force density. An external ac magnetic field of constant frequency is applied to a model superconducting network. By means of the critical state model we have calculated internal field profile in a superconducting network at several temperatures below the critical temperature (9; 12). Unlike Muller, we have assumed a purely ac external magnetic field for simplicity. All field profiles are calculated at a time instant of $t = 0.02$. We have calculated the internal field profile for four grain radii, R_g. The field profiles thus

obtained using different set of parameters have been analyzed. The effect of the grain size on the field profile has been studied. At a fixed pinning force density amplitude the real and imaginary parts of the complex susceptibility have been calculated using grain radius as a parameter. The shifting of the peak in the imaginary part as a function of temperature with the grain radius has been discussed in qualitative way and compared with the shifting caused by the other parameters. The effect of large dc magnetic field on peak temperature has also been studied(20).

2.2 Model

The superconducting sample is modelled as grain-clusters (g) with fixed number of grains per cluster, separated by nongrained regions (J). One nongrained region and one grained region together form one composite segment and all composite segments are of equal lengths. There are five composite segments in each half of the sample. An ac magnetic field in the form of $H = H_m^a cos(\omega t)$ with $H_m^a = 200$ is used externally. The critical state equation of the following form is solved for the magnetic field inside the sample

$$\frac{dH_J(x,t)}{dx} = \pm \frac{1}{\mu_0 \mu_{eff}(T)} \frac{\alpha_J(x,T)}{|H_J(x,t)| + H_{0J}} \tag{2.1}$$

where $|H_J(x,t)|$ is the local field in the nongrained regions at any time instant t. $\alpha_J(x,T)$ is the pinning force density in the same region. Similar critical state equation holds for the superconducting grains. μ_{eff} is the effective permeability of the sample (9). Penetration depth $\lambda(T) = \lambda_0 + (T/T_c)^n; n = 2$ has been assumed. A functional form of the pinning force density $\alpha_{J(g)}(x,T)$ is considered to follow the separation of variables of temperature and position in both g and J regions as given below.

$$\alpha_{J(g)}(x,T) = \alpha_{J(g)0}(x)\left(1 - \frac{T}{T_c}\right)^2 \tag{2.2}$$

We have considered a functional form for the position-dependent pinning force density, $\alpha_{J(g)0}(x)$ following the Gaussian function,

$$\alpha^G_{J(g)0}(x) = \alpha_G e^{-(x-\mu_i)^2/2\sigma^2} \tag{2.3}$$

The Gaussian pinning force density profile is repeated and modelled with a peak located at the midpoint of every nongrained region (J) and σ equal to $1/6th$ of nongrained region length. This ensures low pinning in the grained regions (g) as compared to the nongrained regions, J. Solving the critical state equation we have found the internal field profile for a particular grain radius, R_g. Dependence of the internal field profile on the grain radius has been discussed. Using the field profile we have calculated both the real and imaginary parts of the complex susceptibility

as a function of temperature. We have also investigated the real and imaginary parts as a function of T for several values of R_g.

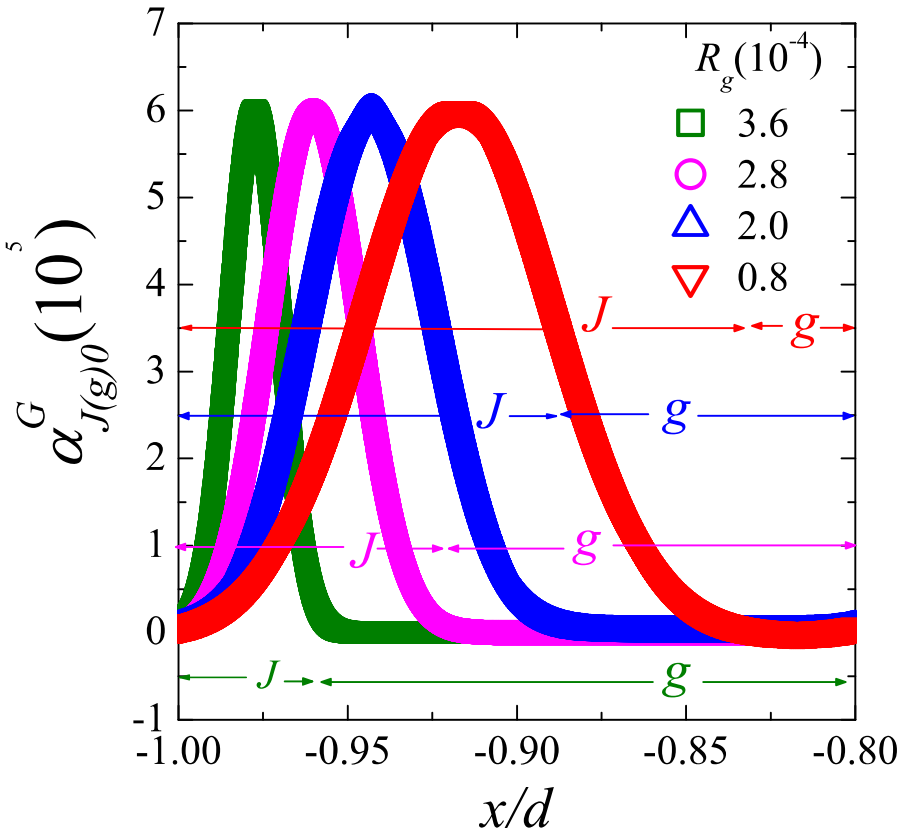

Figure 2.1: The spatial variations in Gaussian pinning force density inside granular superconducting sample for four different grain radius. One nongrained (J) region and one grained (g) region comprising multiple grains with same radius, form one composite segment and is shown in the figure. Each composite segment is 1/10th of total sample length. x/d=-1 corresponds to the edge of the sample whereas x/d=0 is taken as the centre of the sample. Repetitive Gaussian form is obtained by repeating the above variation from x/d=-1 to x/d=+1

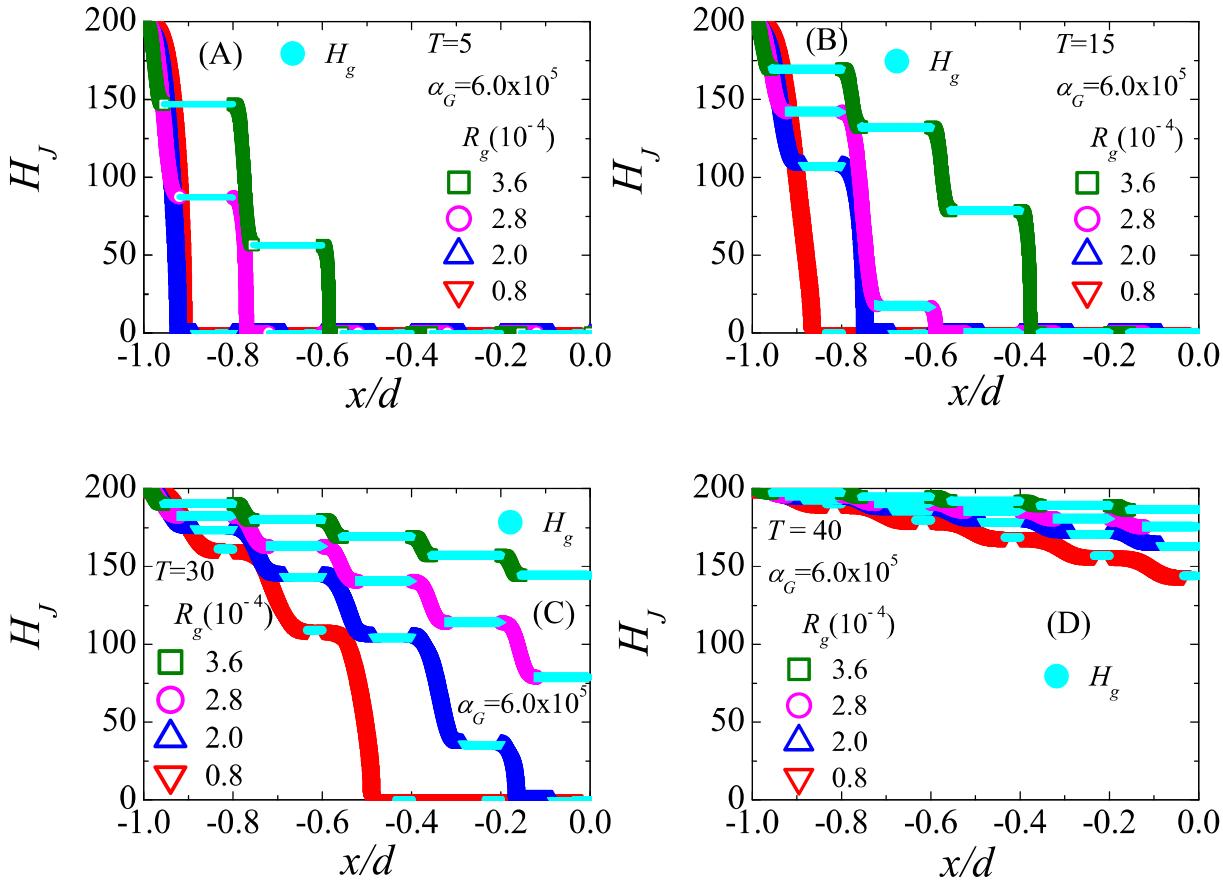

Figure 2.2: (A-D) Variations of the internal field as a function of the position for four grain radii. The pinning profile has the repetitive Gaussian functional form with a maximum of $\alpha_G = 6 \times 10^5$. Panels (A), (B), (C) and (D) correspond to T =5 , 15, 30 and 40 respectively. In each panel the profile in the non-grained region is represented by H_J, and for the grained regions it is given by H_g. H_J and H_g are marked by separate color for a particular grain radius. Four different values of grain radius are included in each panel.

2.3 Results

In Figure 2.1 the variation of the pinning force density with x/d has been shown in the limited range in position for the four different radii of the grains following the Gaussian functional form as given in Equation 3. The first peak of the pinning force density is located at $x/d = -0.98$ for $R_g = 3.6 \times 10^{-4}$, $x/d = -0.96$ for $R_g = 2.8 \times 10^{-4}$, $x/d = -0.94$ for $R_g = 2.0 \times 10^{-4}$, and $x/d = -0.92$ for $R_g = 0.8 \times 10^{-4}$. For each grain radius we have repeated the corresponding pinning force density throughout the entire sample to achieve the total position-dependent pinning profile. The total functional form has been obtained by using Equation 2 in which we used T_c=51. Inserting the total form of $\alpha_{J(g)}(x,T)$ we have calculated the internal field profile H_J and H_g related to J and g regions respectively at a particular time instant $t = 0.02$ (9). In Figure 2.2 (A-D), we have plotted the internal field profiles for T=5, 15, 30 and 40 using same value of $\alpha_G = 6 \times 10^5$. In the panel (A) of Figure 2.2, the field profiles are shown for $R_g = 0.8 \times 10^{-4}$, 2.0×10^{-4}, 2.8×10^{-4} and 3.6×10^{-4} and $T = 5$. The field profile curve consisting of successive H_J and H_g for $R_g = 3.6 \times 10^{-4}$ reveals that there is a nature of penetration which does not follow the exponential nature. The nature of the field profiles for other R_g values also indicates the nonexponential nature of the field-penetration at $T = 5$. The field penetrates maximum distance from the surface ($x/d = -1$) for $R_g = 3.6 \times 10^{-4}$ in comparison to the penetration depths for other

three R_g values. As shown in the panel (A), the internal field becomes zero at certain x/d values which are different for different radii. At T=5, $H_J = 0$ at values of x/d= -0.91, -0.92, -0.77, -0.59 for $R_g = 0.8 \times 10^{-4}$, 2.0×10^{-4}, 2.8×10^{-4} and 3.6×10^{-4} respectively.

In the panel (B) of Figure 2.2, we have shown the field profiles at $T = 15$ for all four grain radius. The penetration of the field is deeper at $T = 15$ for all radii in comparison to that of the depth of the penetration at $T = 5$. For T =15, $H_J = 0$ at values of x/d= -0.87, -0.75, -0.59 and -0.38 for $R_g = 0.8 \times 10^{-4}$, 2.0×10^{-4}, 2.8×10^{-4} and 3.6×10^{-4} respectively. This also indicates that at $T = 15$ several grain clusters in all samples (different R_g) are completely free of field with the zero H_J near the centre of the sample (both sides of x/d=0). For $R_g = 3.6 \times 10^{-4}$, 38 percent of the length the sample remains free of the internal field at $T = 15$.

We have shown the field profiles in panel (C) of Figure 2.2 for $T = 30$ for same set of radii. Interestingly the penetration of the field exhibits that H_J=0 at x/d=-0.48 and -0.16 corresponding to $R_g = 0.8 \times 10^{-4}$, 2.0×10^{-4} respectively. At $T = 30$ and for the grain radius $R_g = 0.8 \times 10^{-4}$, $H_J = 0$ at $x/d = -0.49$ which reveals that only the third, fourth and fifth grain clusters are free of magnetic field. However, for other two higher radii $R_g = 2.8 \times 10^{-4}$ and 3.6×10^{-4}, H_J is finite everywhere. Therefore, at $T = 30$, the shielding in the interior of the sample vanishes for these two values of R_g and complete penetration of the field

is obtained. It is needless to mention that the overall step-like profile also remains unaltered at $T = 30$.

In Figure 2.2(D) we have shown a panel in which the field profile has been shown for $T = 40$. It is clear that at the same time instant $t = 0.02$, the field penetrates upto the centre of the sample for all four R_g. At the center, H_J has the maximum value for the highest $R_g = 3.6 \times 10^{-4}$. In addition, it will be important to mention that there is no normalised position x/d at which H_J=0 at $T = 40$ for all four samples with specific R_g. Therefore, no complete shielding effect has been found even at the center at a higher temperature $T = 40$ close to T_c = 51. However the nonexponential behavior of the field profile remains unaltered in nature (13).

In addition to the above features of the local field profile, the changes in field in the grain free regions (J), ΔH_J becomes steeper with the lowering in the temperature. At $T = 15$, the maximum change in field, $\Delta H_{Jmax} = 200$ for the sample with grain radii $R_g = 0.8 \times 10^{-4}$ in the first grain free region from the surface of the sample. At $T = 30$, $\Delta H_{Jmax} = 108.97$ for $R_g = 0.8 \times 10^{-4}$ in the third grain free region from sample surface. It is important to mention that the change in the field are also much higher in the regions of the sample with no grains, than in the granular regions. Therefore, in presence of the oscillatory pinning force density for all four R_g as shown in Figure 2.1, the corresponding field profiles are nonexponential at all $T < T_c$ (14).

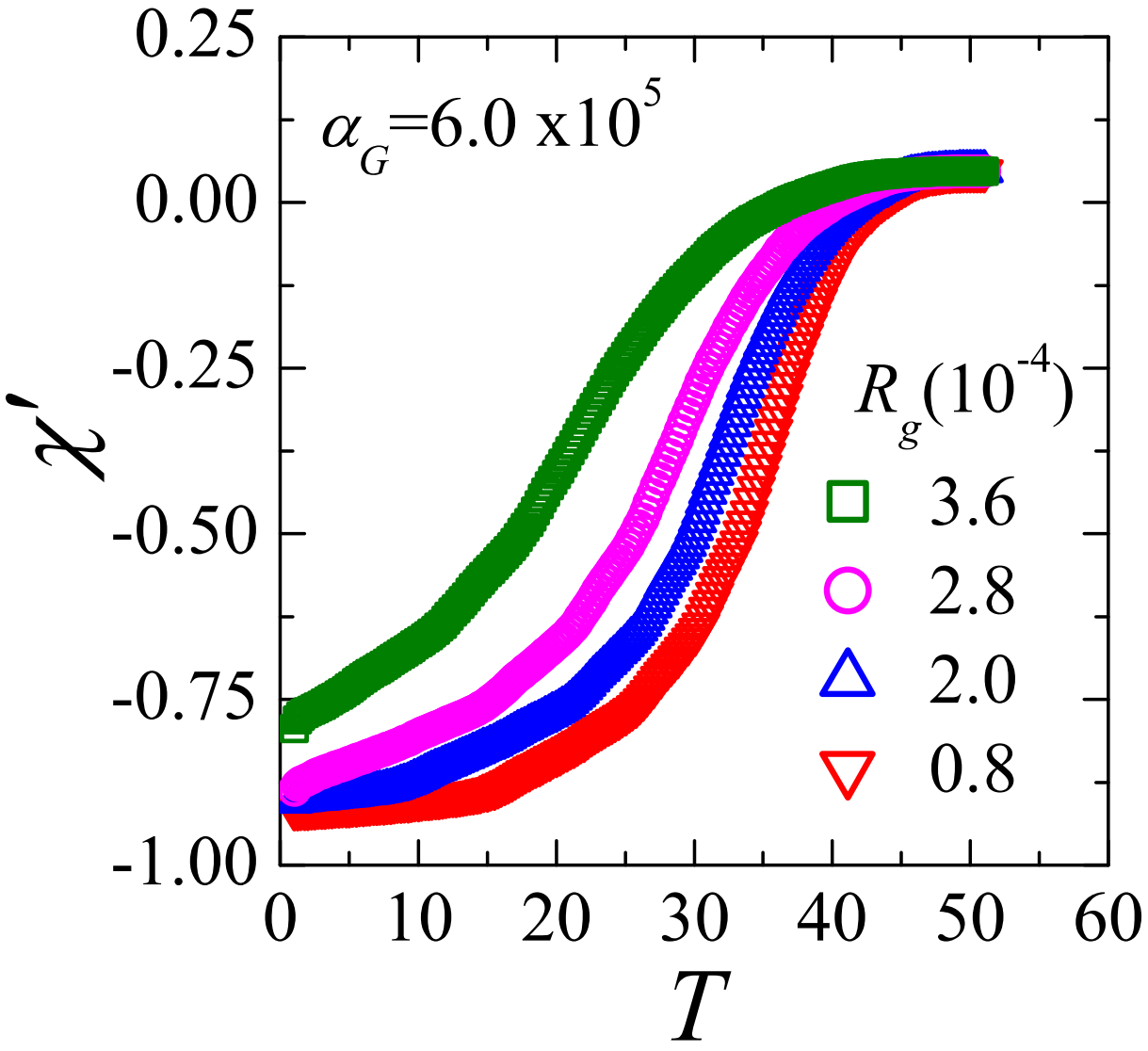

Figure 2.3: Real part of the susceptibility, χ', as a function of temperature for samples with different grain radius.

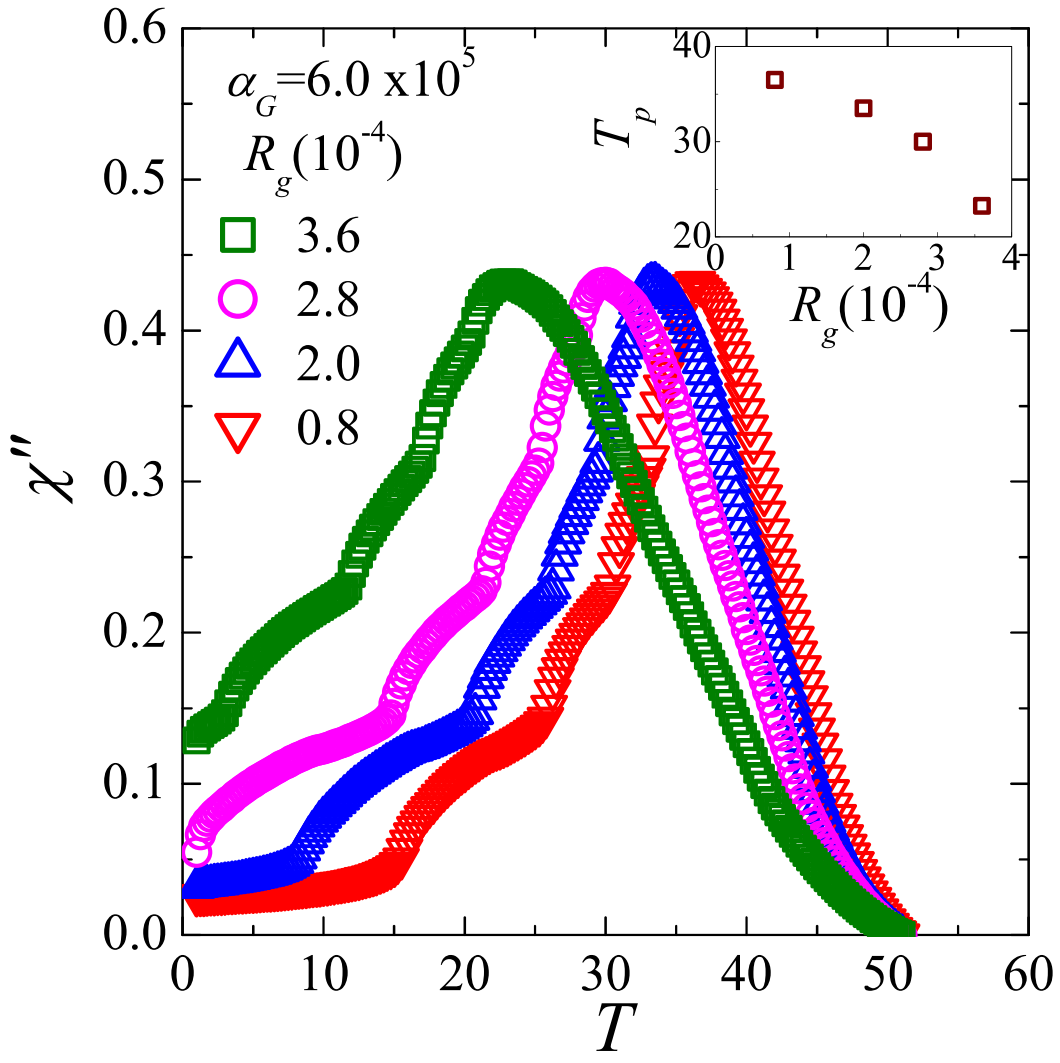

Figure 2.4: Variations of the imaginary part of the ac susceptibility,χ'', as a function of temperature for samples with different grain radius. T_p is the temperature at which $\chi''(T)$ has a peak. In the inset the variation of T_p with R_g has been plotted.

$R_g(10^{-4})$	T_p	χ'' at T_p
0.4	37	0.4318
0.8	36.5	0.4319
1.2	35.5	0.4318
1.6	34.75	0.4318
2	33.5	0.4319
2.4	32	0.432
2.8	30	0.432
3.2	27.25	0.4319
3.6	23.25	0.4319
4.0	15.5	0.4319

Table 2.1: Change in the value of χ'' peak and peak temperature T_p with different grain radii R_g for superconducting samples.

Integrating the field profile across non-grained and grained regions and within limit of the time period of the ac cycle the susceptibility of a sample at a particular temperature has been calculated. In Figure 2.3, we have plotted the variation of the real part of the complex susceptibility, χ', as a function of the temperature. As we increase the radius of the grain, the diamagnetic effect becomes weaker at a particular temperature below T_c (15). The shielding effect becomes weaker as is shown in Figure 2.2 at $T = 5$ for $R_g = 3.6 \times 10^{-4}$ in comparison to that

of sample with $R_g = 0.8 \times 10^{-4}$. It is manifested in the variation of the real part as well. At higher T, the field profile penetrates strongly which results in higher value of χ'. In several superconducting systems, it is observed that $\chi'(T)$ gets affected in similar way as the applied amplitude of the ac field is increased. The change in the variation $\chi'(T)$ with the increase in R_g numerically exhibits analogous changes. Therefore, increasing the grain radius and increasing the amplitude of the ac field in superconductor below the critical temperature show similar effect in $\chi'(T)$ (16). In Figure 2.4, we have shown the variation of the imaginary part with the temperature, $\chi''(T)$. Clearly $\chi''(T)$ depends strongly on R_g. The variation of $\chi''(T)$ has the maximum at the temperature T_p (16; 17). The peak in the $\chi''(T)$ at the temperature (T_p) corresponds to the maximum magnetic loss (18). The critical current decreases with the increase in temperature and the field penetration depth increases with temperature leading to the above peak. The height of the peak shows a negligible change with the change in the grain radii. Moreover, the width of the peak increases with the increase in grain radii. In several cuprate superconducting systems the shifting has been reported with the amplitude of the ac field and it has been attributed to the pinning potential (16). In the inset of Figure 2.4, we have shown the variation of the T_p with R_g.The shifting of the peak temperature, T_p towards the lower temperature is a result of the increase in R_g. Table 2.1 further illustrates this shift in T_p while at the same time, highlighting the negligible change in the value of the χ'' peak. The value of the peak is approx-

imately equal to 0.432 for the different samples irrespective of grain radius. The propagation of the flux front associated magnetic loss is therefore very sensitive to R_g. An analogous effect has been observed in experimental results with the increase in the amplitude of the ac magnetic field (19; 20).

2.4 Summary

The repetitive Gaussian (RG) nature of the pinning force density in four superconductors having a specific radius of grains exhibit the nonexponential nature of the internal magnetic field profile. The field profile is affected competitively by both total pinning force density and superconducting fraction determined by the radius of the grains. With the increase in the temperature, the penetration of the field becomes deeper for any specific radius of the grain. At any temperature below T_c, the penetration becomes deeper with the increase in the radius of the grain. The variation of the imaginary part of the complex susceptibility with the temperature exhibits a peak. The temperature at which the peak is observed shifts to the lower temperature as a result of the increase in the radius of the grain. The grain radius has an analogous effect in the imaginary part of the ac susceptibility as is obtained by changing the amplitude of the ac magnetic field.

References

[1] F. London, and H. London, Proc. of the Royal Soceity A : Mathematical, Physical and Engineering Sciences **149** (1935) 71

[2] C. P. Bean, Rev. Mod. Phys. **36** (1964) 31

[3] J. R. Clem, J. Appl. Phys.50 (1979) 3518.

[4] E. H. Brandt, G. P. Mikitik, Phys. Rev. **B76** (2007) 064526

[5] D.-X. Chen, A. Sanchez, J. Nogues, J. S. Muoz, Phys. Rev. **B 41** (1990) 9510

[6] G. P. Mikitik, J. Low temp. Phys. **36** (2010) 13

[7] M. Xu, D. Shi, R. F. Fox, Phys. Rev. **B 42** (1990) 10773

[8] L. Ji, R. H. Sohn, G. C. Spalding, C. J. Lobb, M. Tinkham, Phys. Rev. **B 40** (1989) 10936

[9] K. H. Muller, Physica C **159** (1989) 717

[10] G. Blatter, M. V. Feigelman, V. B. Geshkenbein, A. I. Larkin, V. M. Vinokur, Rev. Mod. Phys. **66** (1994) 1125

[11] D.-X. Chen, E. Pardo, A. Sanchez, S.-S. Wang, Z.-H. Han, E. Bartolome, T. Puig, X. Obradors, Phys. Rev. **B 72** (2005) 052504

[12] K. H. Muller, S. K. H. Lam, X. L. Wang, S. X. Dou, Phys. Rev. **B 85** (2012) 224516

[13] I. M. Babich, G. P. Mikitik, E. H. Brandt, Phys. Rev. **B 74** (2006) 224501

[14] M. J. Qin, X. X. Yao, Phys. Rev. **B54** (1996) 7536

[15] F. Gomory, P. Lobotka, Solid State Comm. **66** (1988) 645

[16] K.-H. Muller, M. Nikolo, R. Driver, Phys. Rev. **B 43** (1991) 7976

[17] M. G. das Virgens, S. García, M. A. Continentino, L. Ghivelder, Phys. Rev. **B 71** (2005) 064520

[18] J.Z. Sun, M. J.Scharen, L. C. Bourne, and J.R. Schrieffer, Phys. Rev. **B44** (1991) 5275

[19] J. R. Clem, A. Sanchez, Phys. Rev. **B 50** (1994) 9355

[20] R. B. Flippen, Phys. Rev. **B45** (1992) 12498

Chapter 3

Dynamics of Local Magnetic Field Profile in Disordered Superconductors

3.1 Introduction

Magnetic field profile inside a type-II superconductor is a subject of intensive research following Bean's model (1). Following the critical state model several attempts are made to understand the position and time variations of the field profile inside several superconductors having specific geometry. Depending on the combinations of several parameters, e.g. geometry, nature of external field, the magnetic field profile inside any superconductor is calculated (2; 17). Superconductors are modelled assuming granular regions and intergranular regions of different distributions. Both the granular and intergranular local field profiles being functions of position and time contributes to the total susceptibility in a complex way. The penetration of an ac magnetic field inside a superconductor affects both

the real and imaginary parts of the susceptibility (3). It is difficult to map dynamics of the local internal field profiles both experimentally and analytically. However numerically it is possible to understand the field variation even inside a network consisting of both the superconducting grains and normal regions. In cuprate superconductor the field profiles have been numerically estimated following critical state model (4; 5). A shifting of the peak in the imaginary part of the ac susceptibility has been explained (6).

Even though several explanations of the penetration of magnetic field inside a type-II superconductor have been attempted using the critical state model it is not understood how pinning force density can be modelled. Any underlying disorder profile determines the pinning force density which in turn controls the flux pinning and internal field profile. We have used critical state model to understand the field penetration in pnictide superconductors. Two different types of position dependent pinning force densities following (i) repetitive Gaussian and (ii) Rademacher functions (square wave) have been assumed. In the critical state equation, we have also inserted a functional form of the London penetration depth $\lambda(T)$ which is generally found to be very effective for pnictide superconductors. Internal field profiles in the Josephson regions, $H_J(x,t)$ and granular regions $H_g(x,t)$ have been calculated. Real and imaginary parts of the ac susceptibility have been calculated as a function of temperature for both types of pinning landscapes.

3.2 Model

The critical state equation of the superconducting sample is given as

$$\frac{dH_J(x,t)}{dx} = \pm \frac{1}{\mu_0 \mu_{eff}(T)} \frac{\alpha_J(x,T)}{|H_J(x,t)| + H_{0J}} \tag{3.1}$$

where $|H_J(x,t)|$ is the local field in the Josephson regions at any time instant t. $\alpha_J(x,T)$ is the pinning force density in the same region and is assumed to be a function of position and temperature. Similar critical state equation holds for the superconducting grains. The sample is under an external ac magnetic field $H_m^a cos(\omega t)$ at any time instant t. μ_{eff} is the effective permeability of the sample and

$$\mu_{eff}(T) = f_n + f_s \frac{2I_1(R/\lambda(T))}{(R/\lambda(T))I_0((R/\lambda(T))} \tag{3.2}$$

f_n is the fraction of normal material, f_s is the fraction of superconducting grains in the sample, I_0 and I_1 are modified Bessel functions of the first kind. R is the grain radius. The effective permeability depends on the penetration depth. In several pnictide superconductors a particular form of $\lambda(T) = \lambda_0 + (T/T_c)^n; n = 2$ has been successfully used to understand several properties (7; 8). We have also inserted this form of $\lambda(T)$ in the critical state equation to determine the local field profiles.

Microscopic causes of pinning include position dependent changes in transition temperature and mean free path length in disordered media (9; 10). The pinning force density is known to be higher in the disordered regions. In our model we assume that the grain-free Josephson regions have higher pinning force density than grains. Following the temperature dependence of the pinning force density used in cuprates, firstly we express $\alpha_{J(g)}(x,T)$ as follows:

$$\alpha_{J(g)}(x,T) = \alpha_{J(g)0}(x)\left(1-\frac{T}{T_c}\right)^2 \tag{3.3}$$

Position dependent part of the pinning force density $\alpha_{J(g)0}(x)$ has been modelled in two different ways. $\alpha_{J0}(x)$ is considered to be $\alpha^G_{J0}(x)$ for the repetitive Gaussian pinning and $\alpha^s_{J0}(x)$ for Rademacher form of pinning. $\alpha_{g0}(x)$ is expressed as $\alpha^G_{g0}(x)$ and $\alpha^s_{g0}(x)$ for the repetitive Gaussian (RG) pinning and the Rademacher form (RD) of pinning respectively. For the Rademacher form of pinning $\alpha^s_{J0}(x) = \alpha_s$ and $\alpha^s_{g0}(x) = 0$. We have used the repetitive Gaussian pinning function as follows:

$$\alpha^G_{J(g)0}(x) = \alpha_G e^{-(x-\mu_i)^2/2\sigma^2} \tag{3.4}$$

where μ_i are the peak positions and total to the number of non-grained separations between the grain clusters in half sample. $x = \mu_i$ for x at midpoint of Josephson regions. Here $x \neq \mu_i$ for any x in the grain clusters. Successive integration of local field in Josephson region, $H_J(x,t)$, and the local field inside grains, $H_g(x,t)$, over sample length and time period is used to numerically determine the susceptibility

of the sample.

3.3 Results

In Figure 3.1, we have shown the variation of internal field profiles $H_J(x)/H_m^a$ and $H_g(x)/H_m^a$ with $H_m^a = 200$, corresponding to the intergranular regions and regions with grains respectively at a particular time instant $t = 0.02$ and $T = 40$, as a function of normalised position x/d for two different average radii (i) $R = 4 \times 10^{-5}$ and (ii) $R = 4 \times 10^{-4}$. For $R = 4 \times 10^{-5}$ values taken for the fractions $f_n = 0.914$ and $f_s = 0.086$. Positions of peaks in RG pinning form shift inwards, towards the centre of the sample with decrease in grain radii. At the centre of the sample $x/d = 0$, the internal field H_g is higher for $R = 4 \times 10^{-4}$. Net pinning force increases with decrease in grain radii, and hence superconducting fraction, in the sample. This results in a higher change in magnetic field in the interior of the sample.

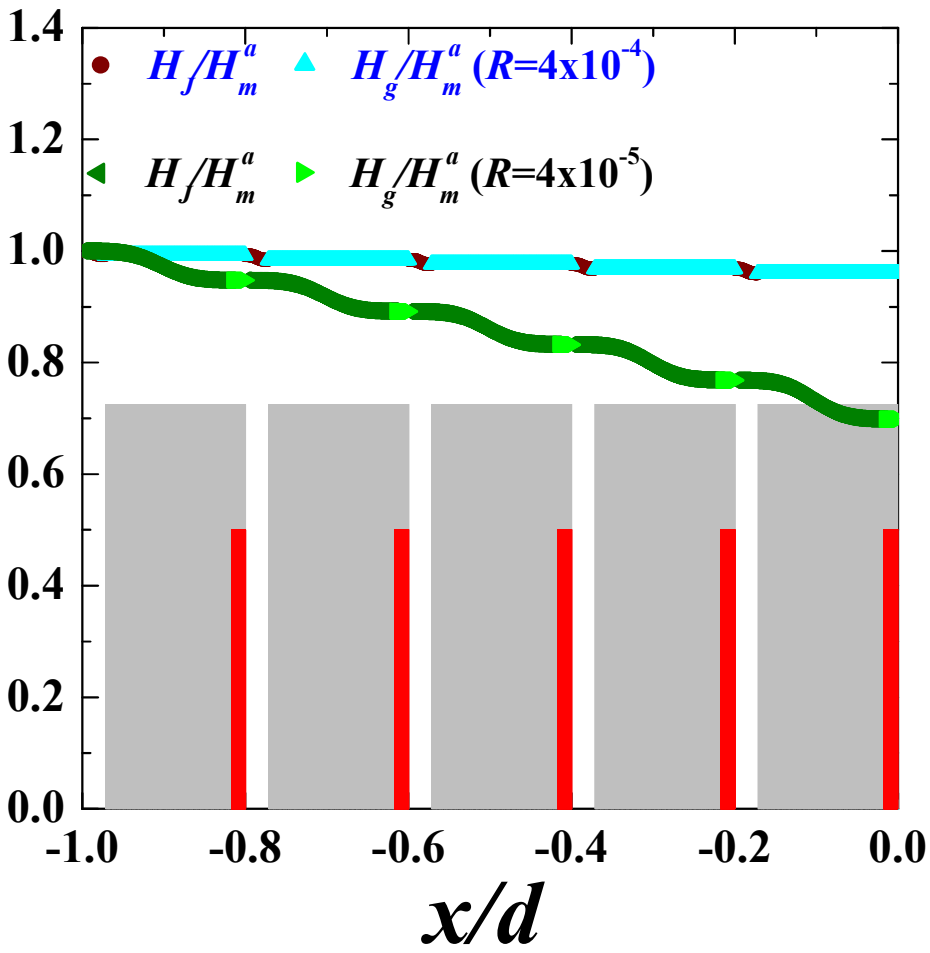

Figure 3.1: A schematic diagram showing the variation of local field profile H_g/H_m^a and H_J/H_m^a in both grainfree regions and grain clusters, along with position of the grain cluster as a function of the normalised position x/d where x/d=-1 represents one of the edges of the sample and x/d=0 represents midpoint of the sample. For grain radii of $R = 4 \times 10^{-4}$, the grain cluster is marked with a higher nominal value 0.725 as compared to the nominal value of 0.5 marking the grain cluster with grain radius 4×10^{-5}. The number of grains in each cluster is $nogs = 215$. Internal magnetic fields are shown for $T = 40$, $t = 0.02$ and with $\alpha_G = 577600$.

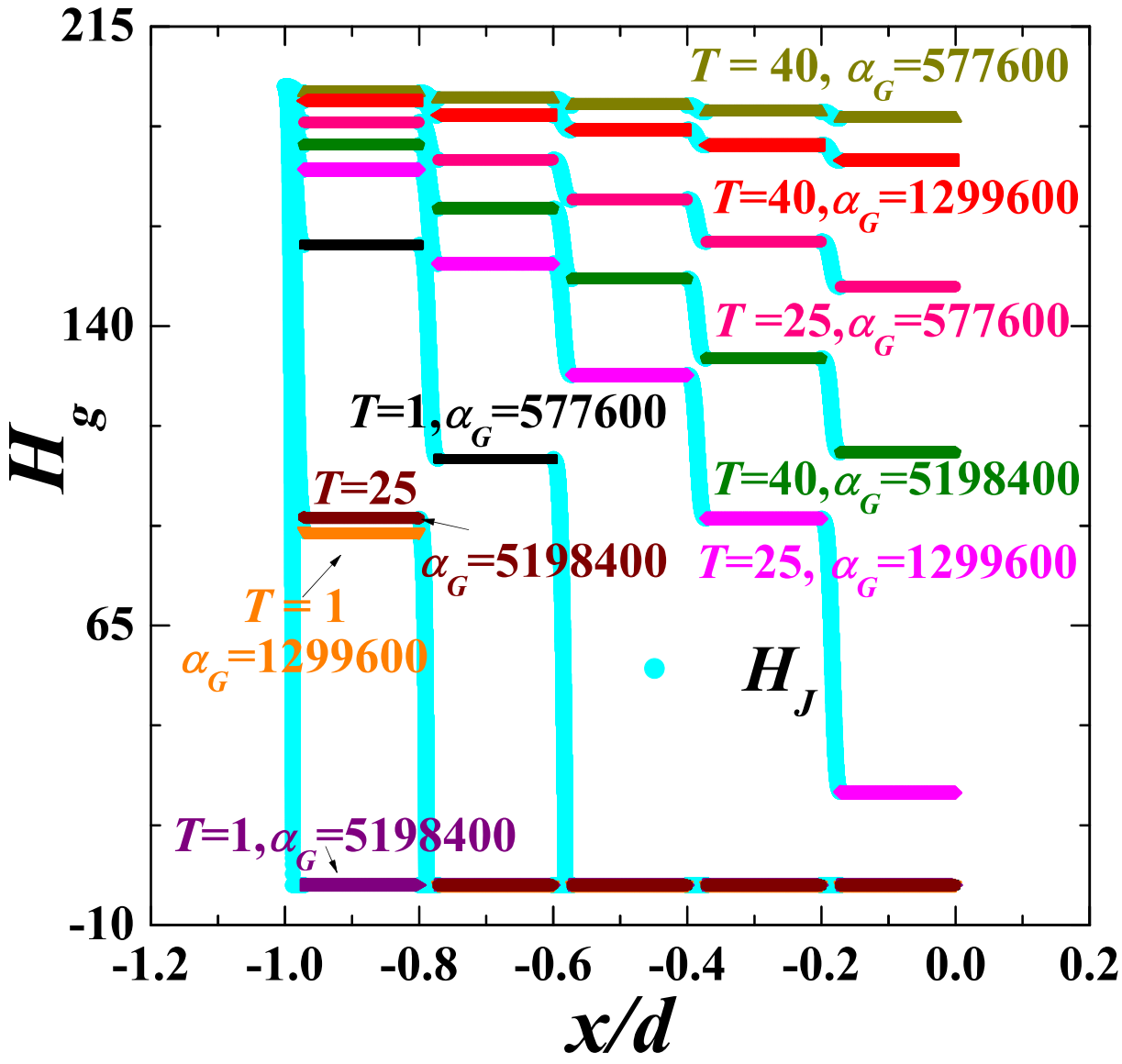

Figure 3.2: Variation of the granular magnetic field H_g as a function of x/d at three temperatures $T = 40, 25$ and 1 for average grain radii $R = 4 \times 10^{-4}$. For all values of T we have used three different RG pinning parameter $\alpha_G = 577600, 1299600$ and 5198400. All variations of H_g correspond to the time instant $t = 0.02$. The variations of internal magnetic field between any two grain clusters, H_J, with x/d have been shown for all these set of parameters.

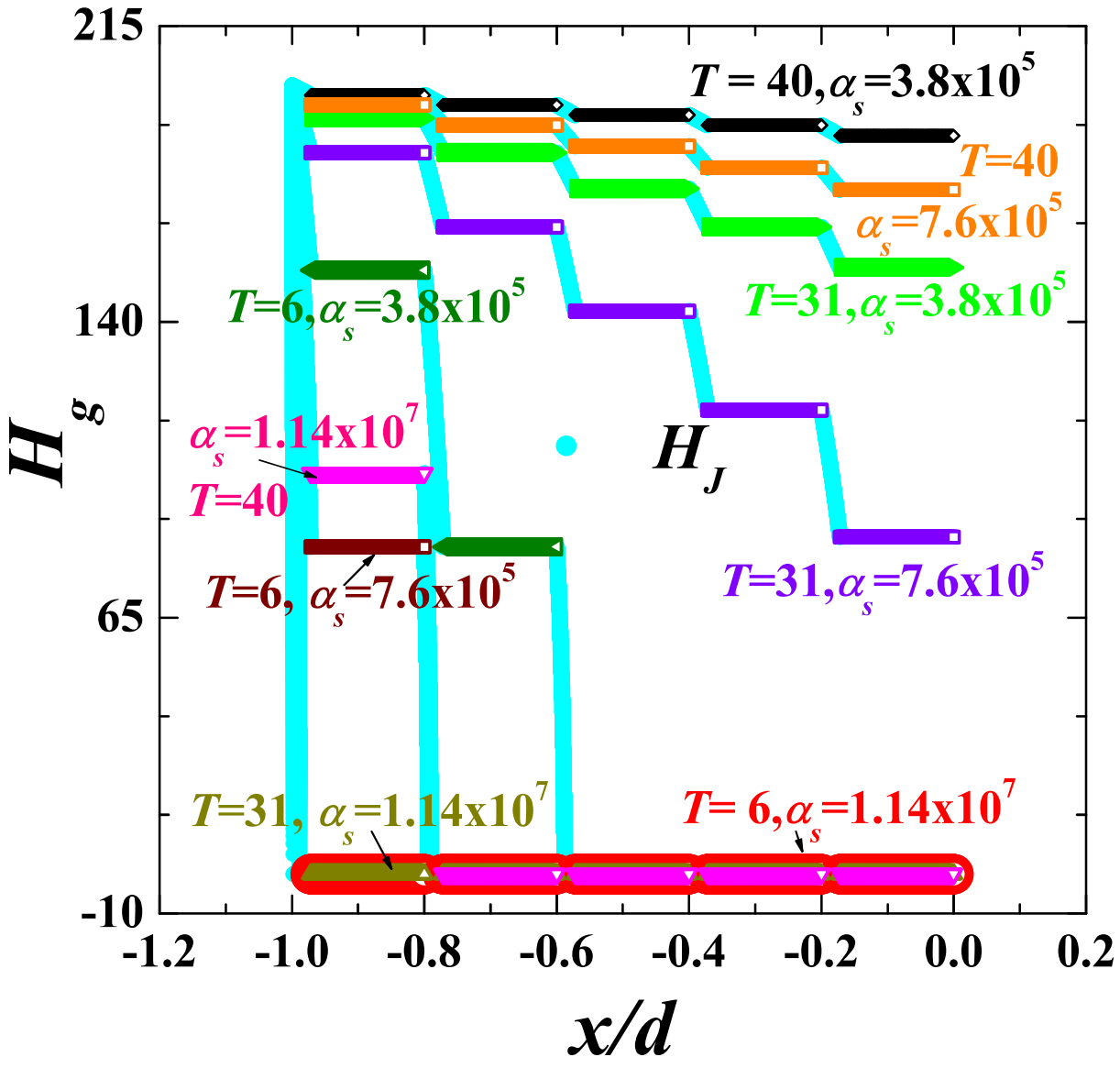

Figure 3.3: Variation of the granular magnetic field H_g as a function of x/d at three temperatures $T = 40, 31$ and 6 for the average grain radii $R = 4 \times 10^{-4}$. For all values of T we have used three different RD pinning parameter $\alpha_s = 3.8 \times 10^5, 7.6 \times 10^5$ and 1.14×10^7. All variations of H_g correspond to the time instant $t = 0.02$. The variations of internal magnetic field between any two grain clusters, H_J, with x/d have been shown for all these cases.

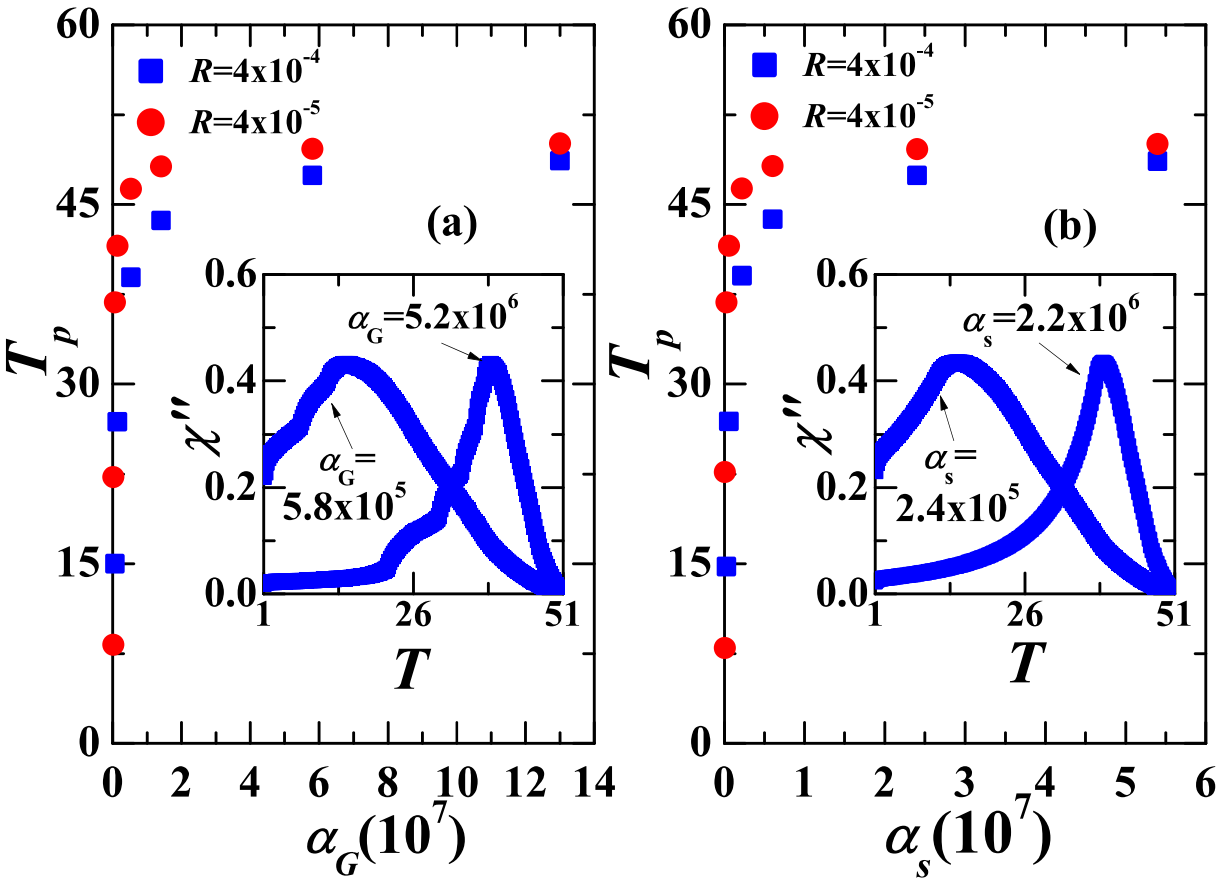

Figure 3.4: Variation of T_p as a function of pinning force densities α_G for the sample with RG pinning (a). In the inset of panel (a) the variation of the imaginary part of ac susceptibility $\chi''(T)$ has been shown, for $R = 4 \times 10^{-4}$. In the inset of panel (b) we have shown the variation of $\chi''(T)$ for two α_s, for $R = 4 \times 10^{-4}$. Variation of T_p with α_s has been shown in panel (b).

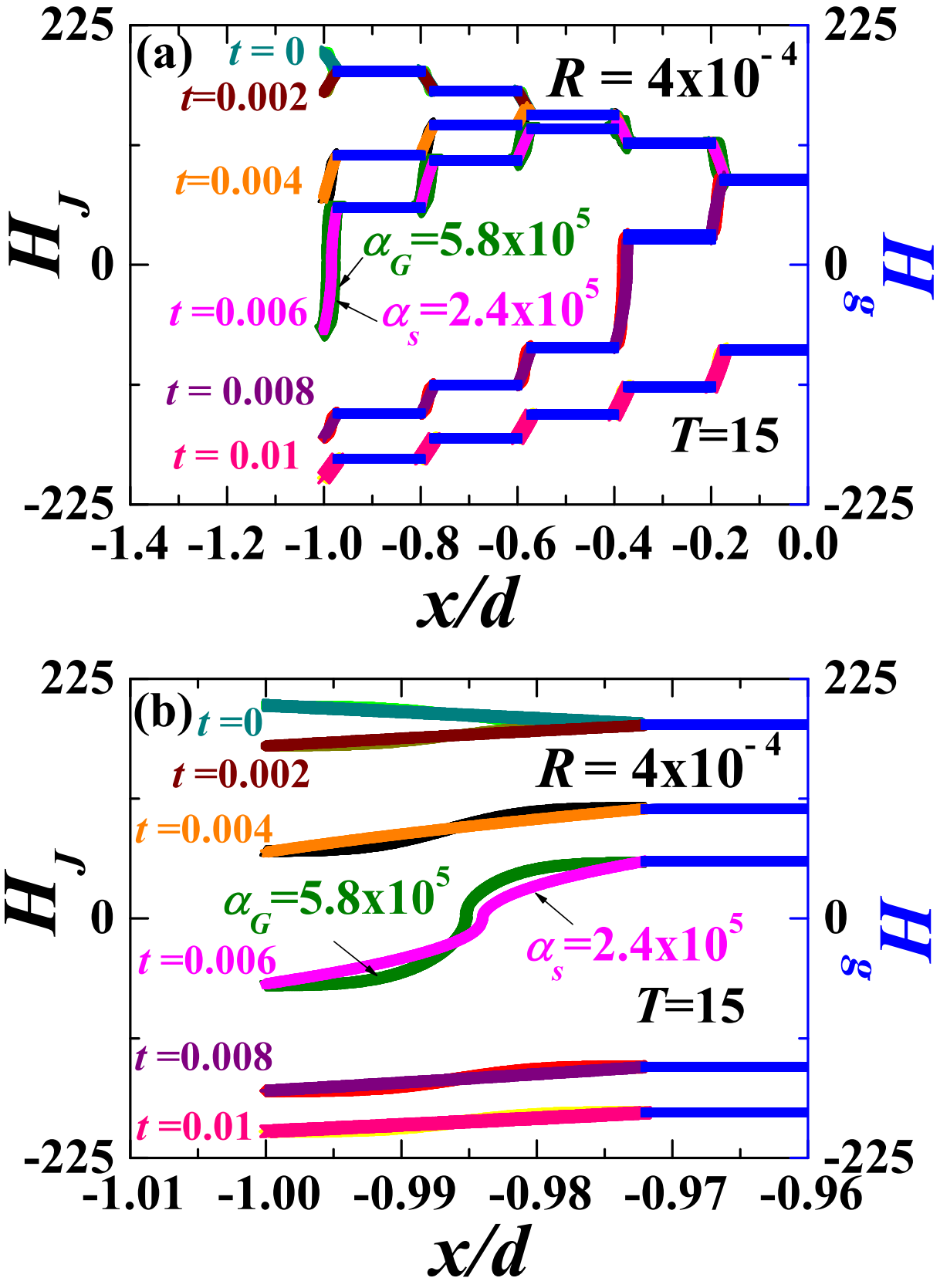

Figure 3.5: (a) Variations of H_J and in grains H_g as a function of x/d at different time t for temperature $T = 15$. (b) Magnified variations of H_J at several time instant.

In Figure 3.2, we have plotted the variations of H_g and H_J as a function of x/d for the RG pinning in sample with $R = 4 \times 10^{-4}$. At any constant T we have shown H_g for three values for $\alpha_G = 577600, 1299600$ and 5198400. At $T = 40$, as we increase α_G, H_g decreases with x/d in the inner part of the sample. Step like features are visible for all three α_G. At a lower $T = 25$, H_g vanishes at $x/d > -0.8$ for α_G = 5198400. At a further lower temperature, $T = 1$, H_g vanishes at $x/d > -0.6$ for all 3 different values of α_G.

In Figure 3.3, we have shown variations of H_g as a function of x/d for the pinning profile following RD in sample with $R = 4 \times 10^{-4}$ at a time instant $t = 0.02$. At a constant $T = 40$ we have used three values of pinning force density parameter, $\alpha_s = 3.8 \times 10^5, 7.6 \times 10^5$ and 1.14×10^7. With the increase in α_s, the penetration of field weakens. For the lowest α_s clear staircase like structure is visible with very high H_g even at the middle of the sample. As we further increase α_s to 7.6×10^5, the overall variation of H_g remains similar with a lower value in the middle of the sample. However, for $\alpha_s = 1.14 \times 10^7$, $H_g = 0$ for the region with $x/d > -0.8$. At other two temperatures $T = 31$ and $T = 6$, the variations are also plotted in Figure 3.3. Interestingly, at $T = 31$ and $\alpha_s = 1.14 \times 10^7$, no field penetrates inside any grain cluster, $H_g = 0$.

To understand the variation of H_J we have extracted rise height, ΔH_J in the Josephson region between any two superconducting grain clusters. For RG pin-

ning ΔH_J increases towards the middle of the sample ($x/d = 0$) for several combinations of T and α_G as shown in Figure 3.2. At $T = 25$ and α_G =1299600, the enhancement of ΔH_J is from 20.77 to 68.35 towards the midpoint of the sample. As shown in Figure 3.3 for the RD pinning the maximum ΔH_J = 32.20 has been obtained in the middle of the sample for a combination of $T = 31$ and $\alpha_s = 7.6 \times 10^5$. Therefore, overall distributions of rise height in both (i) RG and (ii) RD cases have analogous nature but are different in magnitude.

Following equations for the field profiles we have calculated the real and imaginary parts of the ac susceptibility for both (i) RG and (ii) RD nature of pinning force densities. In the inset of Figure 3.4(a) we have plotted the variation of the imaginary part of the ac susceptibility χ'' with temperature for two α_G as representatives related to the RG nature. Clearly there is a peak in χ'' (T) at a temperature T_p which varies strongly with α_G. However, the peak height in $\chi''(T)$ remains unchanged. In Figure 3.4(a), we have plotted variations of T_p with α_G for two values of R. An increase in T_p with α_G is obtained with saturation for higher α_G. For RD type of pinning force densities we have shown variations of χ'' (T) for two different α_s as representatives in the inset of Figure 3.4(b). An increase in T_p with α_s has been obtained as shown in Figure 3.4(b). Therefore, the shifting in the peak temperature remains similar in nature irrespective of the nature of pinning force density.

In Figure 3.5(a), we have plotted the variation of H_J and H_g for both types of the pinning force density with (i) $\alpha_G = 5.8 \times 10^5$ and (ii) $\alpha_s = 2.4 \times 10^5$ and the plot is shown over a range of $x/d = -1$ to $x/d = 0$ at different time instants. Combinations of H_g and H_J changes with t which has been shown in a range of $t = 0$ through $t = 0.01$ using a step of 0.002. Almost comparable pattern of variations of staircase like behavior are visible. In panel (b) of Figure 3.5, we have plotted a magnified variation of H_g and H_J as a function of x/d at several instants of time t. We can see that the internal field H_J changes sharply near the midpoint of the Josephson region, most prominently at time $t = 0.006$. In Figure 3.6 we can see the differences in local field profile more clearly for the two different functional forms of pinning force density at one time instant $t = 0.006$.

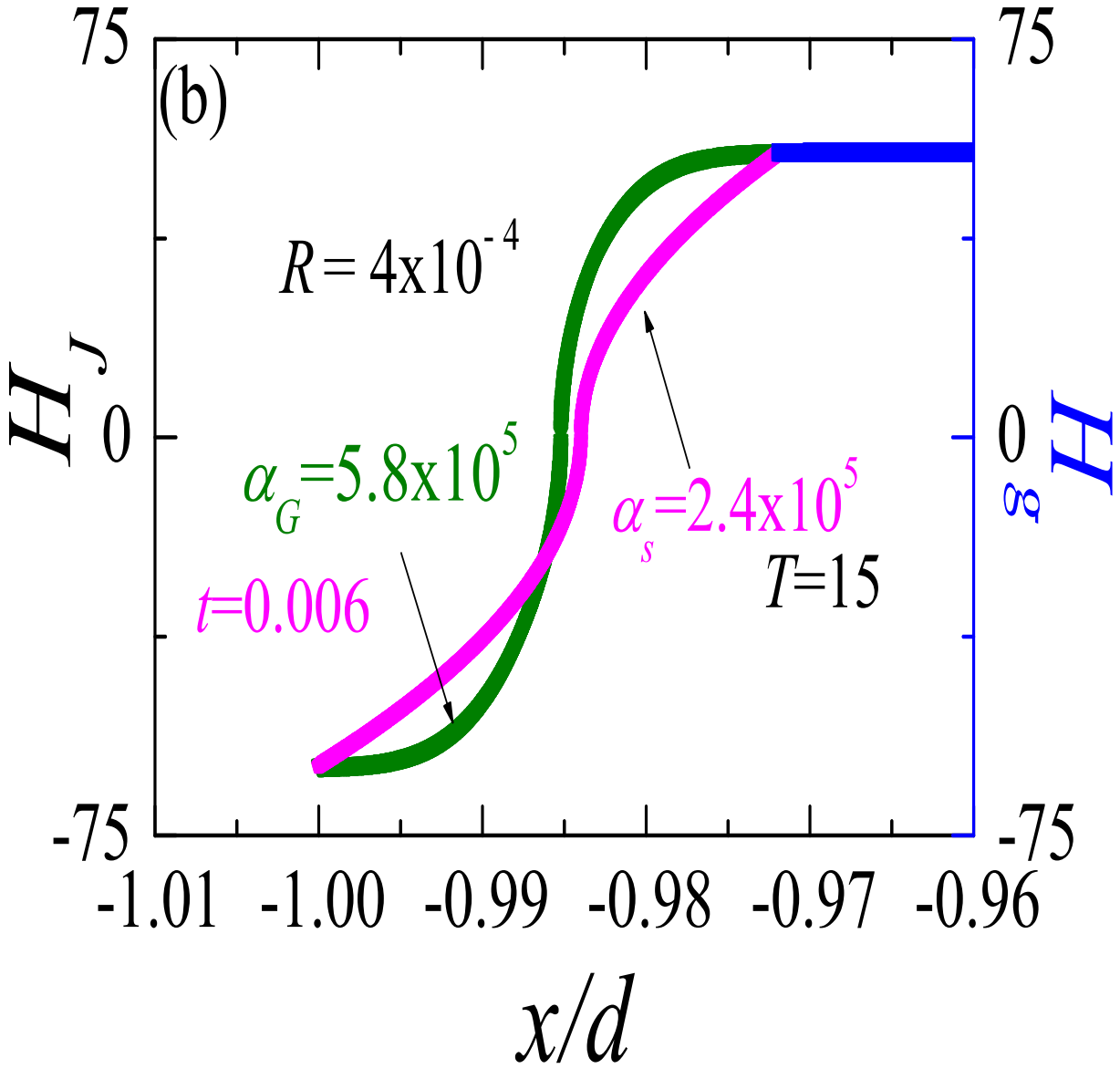

Figure 3.6: Local field profile at time t=0.006 in the first grain-free region and part of the grain cluster

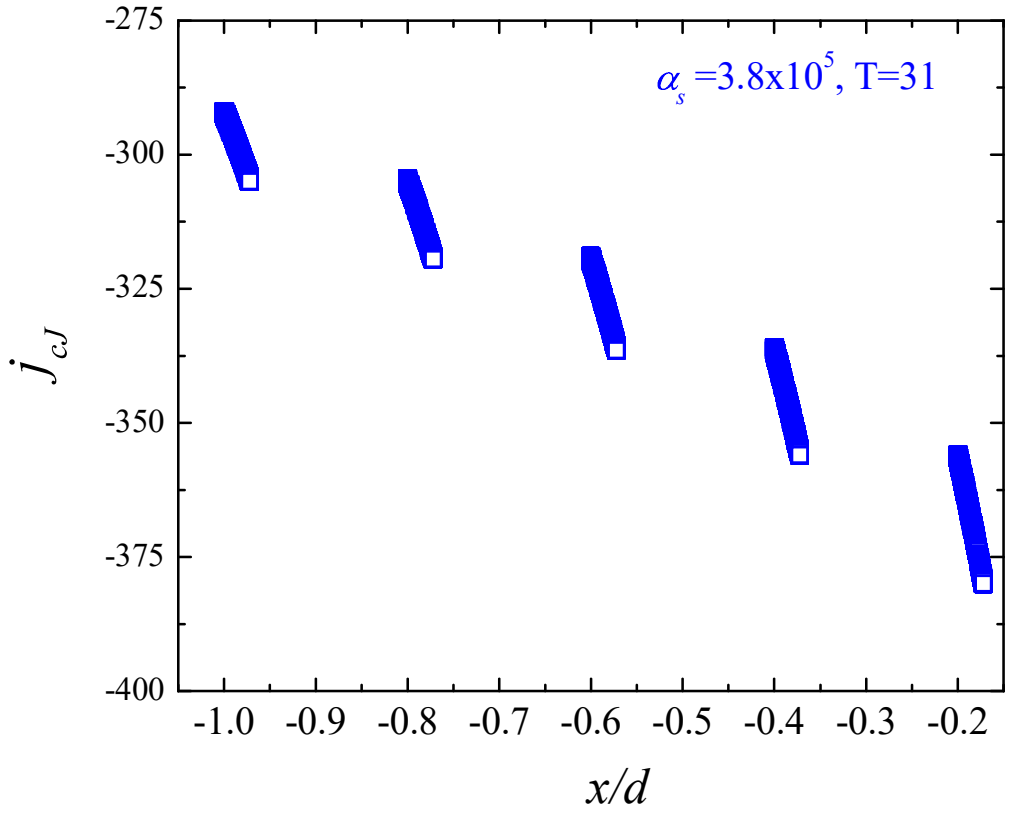

Figure 3.7: Critical current density j_{cJ} in grain free regions in sample with $R = 4 \times 10^{-4}$ and RD pinning constant $\alpha_s = 3.8 \times 10^5$ at $T = 31$

Local critical current density $j_{cJ}(x,t)$ in the superconducting sample can be calculated from the local magnetic field $H_J(x,t)$ in grain-free regions (4) according to the following equation

$$\pm j_{cJ}(x,t) = \frac{dH_J(x,t)}{dx} \tag{3.5}$$

In Figure 3.7 we can see the increase in magnitude of the critical current in the grain-free regions towards the centre of the sample at time $t = 0.02$. The critical current is uniformly zero in the grain-clusters and this results in uniform value of field across these regions.

3.4 Conclusion

Locally critical current density is determined by the ratio of the total pinning force density and the magnetic field at that point in the sample. For RD pinned sample, the field decreases from the surface whereas pinning force density remains the same across the non-grained region. For the RG pinned sample, the field decreases from the surface but the pinning force density increases initially. Comparison between the field profiles in samples with different pinning illustrates the local dependence of magnetic properties of the sample on the pinning profile. At $t = 0.006$, we can clearly see that though the local field profile is not identical throughout the non-grained region, the values of the magnetic field at the surface

and at the beginning of the grain cluster are nearly equal. Comparison between the susceptibility vs temperature graphs of the two differently pinned samples illustrates the global dependence of the magnetic properties of inhomogeneous superconductors on pinning profiles. The peak temperature, T_p increases with the increase in the pinning force density in samples irrespective of the functional form. For sample with Rademacher pinning and $R = 4x10^{-4}$, T_p varies from 14.75 to 48.63 for change in magnitude of pinning constants (α_s) from $2.4x10^5$ to $5.4x10^7$. The difference between the peak temperatures for samples with different radii decreases with increase in pinning magnitude. This difference in T_p for RD pinned samples varies from about 7 for $\alpha_s = 2.2x10^6$ to about 1 for $\alpha_s = 5.4x10^7$. As in (26), the temperature T_p corresponding to χ'' peak, has lower value for higher grain radii.

References

[1] C. P. Bean, Rev. Mod. Phys. **36**, 31 (1964).

[2] E. H. Brandt, Phys. Rev. Lett. **67**, 2219 (1991).

[3] F. Gomory, Supercond. Sci. Technol. **10**, 523 (1997).

[4] K. H. Muller, Physica C 159, 717 (1989).

[5] K. H. Muller, Physica C 168, 585 (1990).

[6] K. H. Muller, S. K. H. Lam, X. L. Wang, and S. X. Dou, Phys. Rev. B **85**, 224516 (2012)

[7] P. J. Hirschfeld and N. Goldenfeld, Phys. Rev. B **48**, 4219 (1993).

[8] R. Prozorov and V G Kogan, Rep. Prog. Phys. **74**, 124505 (2011).

[9] R. Griessen, Wen Hai-hu, A. J. J. van Dalen, B. Dam, J. Rector, H. G. Schnack, S. Libbrecht, E. Osquiguil, and Y. Bruynseraede, Phys. Rev. Lett. **72**, 1910 (1994).

[10] G. Blatter, M. V. Feigel'man, V. B. Geshkenbein, A. I. Larkin, and V. M. Vinokur, Rev. Mod. Phys. **66**, 1125 (1994).

[11] M. Strongin, D. G. Schweitzer, A. Paskin, and P. P. Craig, Phys. Rev. **136**, A926 (1964).

[12] M. Daumling and D. C. Larbalestier, Phys. Rev. B **40**, 9350 (1989).

[13] J. R. Clem, Phys. Rev. B **43**, 7837 (1991).

[14] J.Z. Sun, M. J.Scharen, L. C. Bourne, and J.R. Schrieffer, Phys. Rev. B **44**, 5275 (1991).

[15] X. C. Jin, Y. Y. Xue, Z. J. Huang, J. Bechtold, P. H. Hor, and C. W. Chu, Phys. Rev. B **47**, 6082 (1993).

[16] E. H. Brandt and M. Indenbom, Phys. Rev. B **48**, 12893 (1993).

[17] S. Shatz, A. Shaulov, and Y. Yeshurun, Phys. Rev. B **48**, 13871 (1993).

[18] E. H. Brandt, Phys. Rev. B **54**, 4246 (1996).

[19] M. J. Qin and X. X. Yao, Phys. Rev. B **54**, 7536 (1996)

[20] M. Konczykowski, C. J. van der Beek, M. A. Tanatar, H. Luo, Z. Wang, B. Shen, H. H. Wen and R. Prozorov, Phys. Rev. B **86**, 024515 (2012).

[21] B. Raes, J. Van de Vondel, A. V. Silhanek, C. C. de Souza Silva, J. Gutierrez, R. B. G. Kramer, and V. V. Moshchalkov, Phys. Rev. B **86**, 064522 (2012).

[22] M. Vanevic, Z. Radovic, and V. G. Kogan, Phys. Rev. B **87**, 144501 (2013).

[23] R. T. Gordon, C. Martin, H. Kim, N. Ni, M. A. Tanatar, J. Schmalian, I. I. Mazin, S. L. Bud'ko, P. C. Canfield, and R. Prozorov, Phys. Rev. B **79**, 100506R (2009);

[24] R. G. Mints and A. L. Rakhmanov, Rev. Mod. Phys. **53**, 551 (1981).

[25] C. Reichhardt and C. J. Olson Reichhardt, Phys. Rev. B **76**, 064523 (2007).

[26] S. Roy and A. K. Ghosh, Physica C **580**, 1353766(2021)

Chapter 4

Complex susceptibility in Repetitive Gaussian and Rademacher pinned 2D samples with low anisotropy

4.1 Introduction

Critical State Equation has been successfully used to model superconducting samples of quasi one-dimensional shape assuming different functional dependence of critical current on magnetic field. Exponential and inverse field dependent critical current and field-independent critical current have been used to explain magnetic properties of superconducting samples under different conditions. Importance of sample geometry on magnetic field response of samples have been observed experimentally and numerically. Various methods have been used to apply critical state model to samples with quasi 2D geometries by considering samples with three unequal dimensions and width much less than length much less than height (2). Trends in Lorentz force acting on flux lines are also calculated by consid-

ering the interaction of individual vortex line with pinning microstructure (1). Molecular Dynamics models have also been used to obtain magnetic properties of superconductors (4)

We have undertaken 2D extension of the model as a step towards the understanding of more complicated and more realistic sample geometry, defect geometry and hence pinning due to such defects. 2D extension of the model is undertaken under the assumption of independent, decoupled pinning properties along the two directions of the sample perpendicular to the applied field. Qualitative comparison of changes in susceptibility with temperature between the 1D and 2D models is undertaken.

4.2 Model for 2D

Keeping with the 1D model (12), we consider both Rademacher and Gaussian distributions for spatial variations in pinning profile of the sample. x and y directions are considered identical in size and in pinning distributions and perpendicular to the incident magnetic field. Solving the critical state equation independently along both axes and integrating local fields along spatial extension of the sample and time period of the ac field, we calculate the magnetic susceptibility of the

sample. Critical state equations in 2D case are given as:

$$\frac{dH_J(x,t)}{dx} = \pm \frac{1}{\mu_0 \mu_{eff}(T)} \frac{\alpha_J(x,T)}{|H_J(x,t)| + H_{0J}} \tag{4.1}$$

$$\frac{dH_J(y,t)}{dy} = \pm \frac{1}{\mu_0 \mu_{eff}(T)} \frac{\alpha_J(y,T)}{|H_J(y,t)| + H_{0J}} \tag{4.2}$$

where $\alpha_J(x,T) = \alpha_J(y,T)$ for $x = y$.

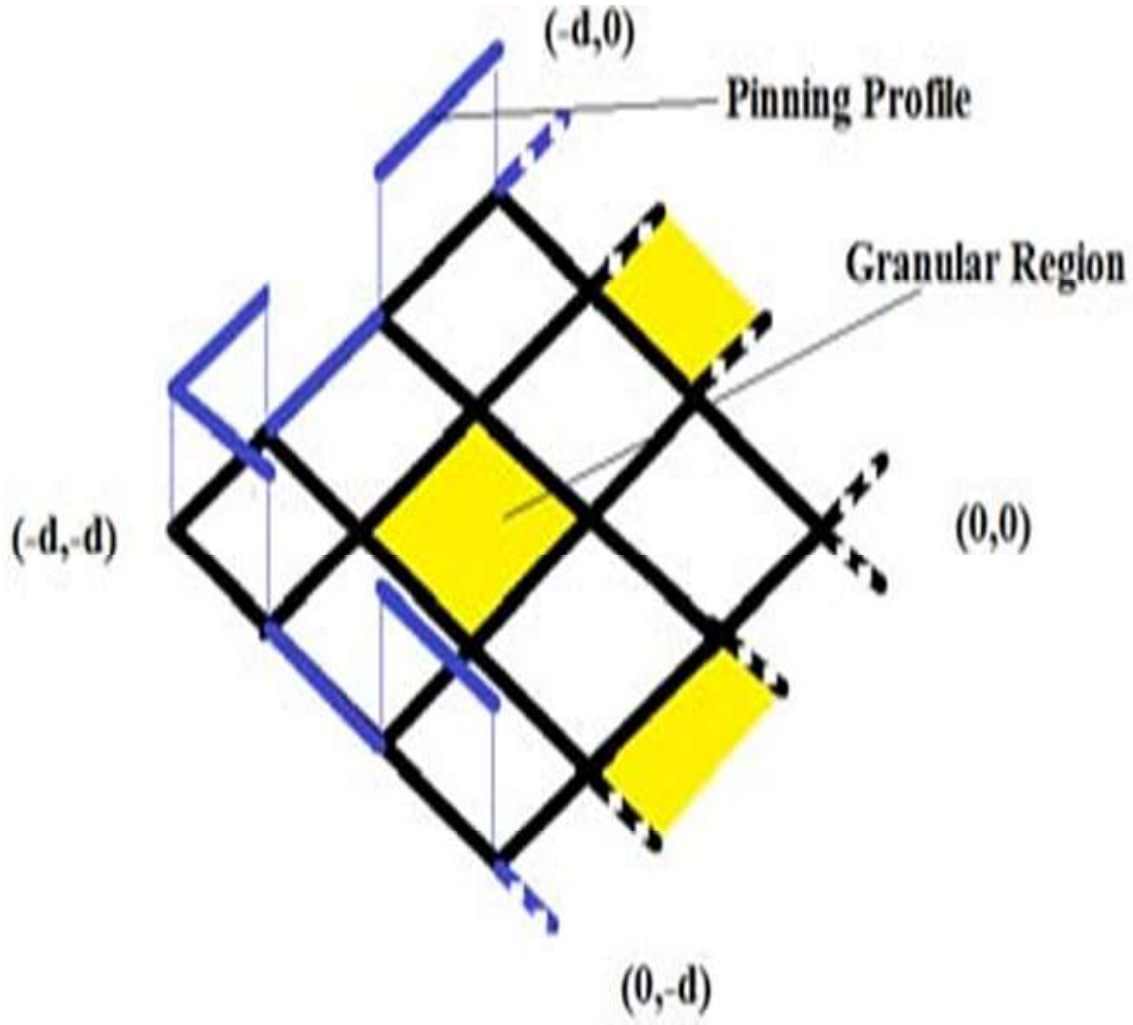

Figure 4.1: Schematic of 2D RD pinned sample

In Figure 4.1, a diagrammatic representation of two dimensional Rademacher pinned sample is shown. Pinning force density along each axis is either a non-zero constant or zero. This leads to the formation of four distinct zones with zero pinning force density along both x and y axis, maximum pinning along both directions, or zero pinning along one axis and constant pinning along the other axis. Our model assumes superconducting grains to be present only in the zone where pinning is zero along both directions. Unlike the representative figure, the length of the non-zero and zero pinning segments are not always equal. This leads to different fractions of superconducting grains f_s calculated by the following equation

$$f_s = \left(\frac{nogs \times 2R \times noseg}{d} \right)^2 \tag{4.3}$$

where $nogs^2$ is the number of grains in each grain-cluster zone; $noseg$ is the number of alternating constant and zero magnitude pinning force density segments along each axis.

4.3 Results and Discussions

Superconducting fraction of 0.0462 to 0.7396 corresponding to a minimum grain radii of $R = 1\text{x}10^{-4}$ and a maximum grain radii of $R = 4\text{x}10^{-4}$, is probed under this model for both Rademacher pinned and Repetitive Gaussian pinned 2D samples.

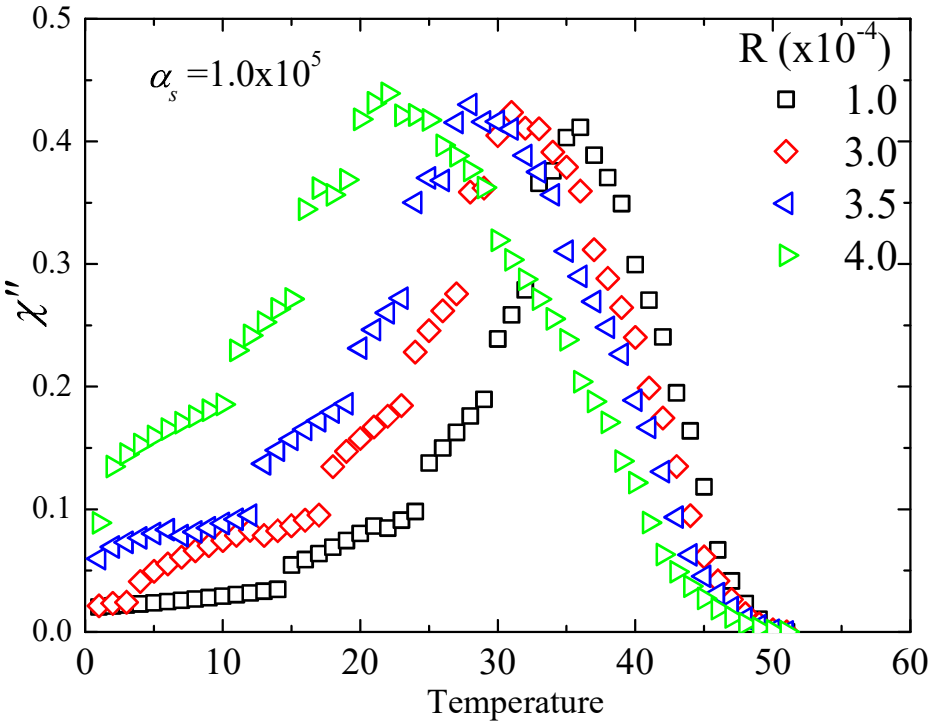

Figure 4.2: χ'' *vsT* graph for RD pinning in 2D. Clear changes in slope visible for $T < T_p$, unlike the 1D scenario for the same pinning profile sample.

Peak temperatures show a similar trend of increase to higher values with decrease in grain radii as compared to the one dimensional case. $T_p = 36$ and 22 for RD pinned 2D sample with $R/d = 1x10^{-4}$ and $4x10^{-4}$ respectively and $\alpha_s = 1x10^5$ as can be seen in Figure 4.2. T_p also increases with increase in magnitude of pinning potential.

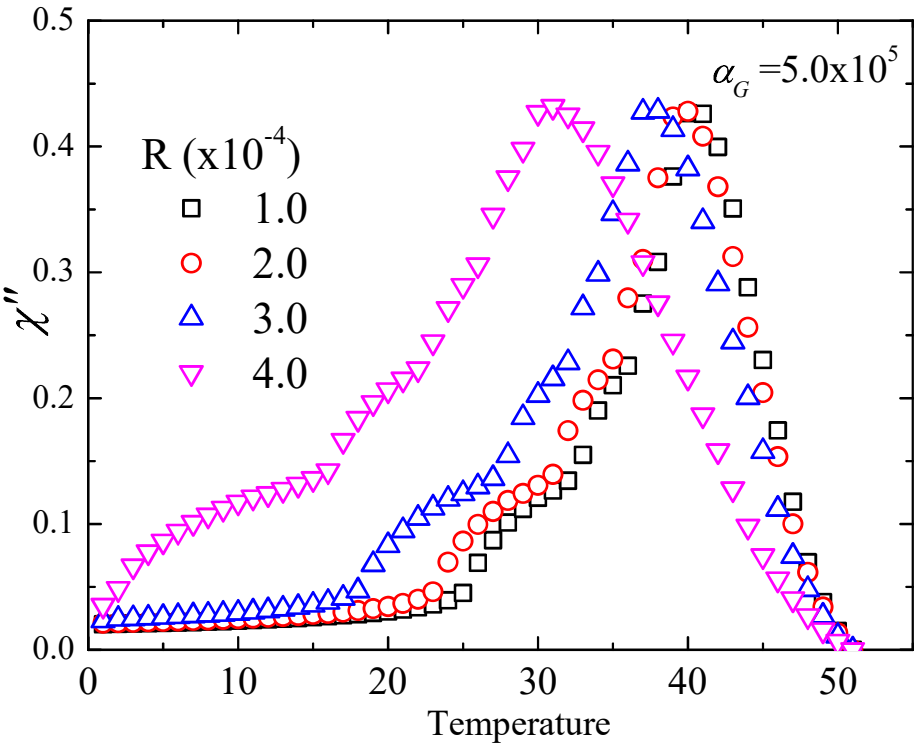

Figure 4.3: $\chi''vsT$ graph for Gaussian pinning constant $\alpha_G = 5.0 \times 10^5$, different radii.

$R(10^{-4})$	f_s	T_p	χ'' at T_p
1.0	0.0462	40	0.426
2.0	0.1849	40	0.428
3.0	0.416	38	0.428
4.0	0.7396	31	0.432

Table 4.1: Change in the value of χ'' peak and peak temperature T_p with different grain radii R and superconducting fraction f_s for RG pinned superconducting samples with $\alpha_G = 5.0\text{x}10^5$

$T_p = 40$ and 31 for RG pinned 2D sample with $R/d = 1x10^{-4}$ and $4x10^{-4}$ respectively and $\alpha_G = 5x10^5$ as can be seen in Figure 4.3. From Table 4.1, we can see that the value of peak $\chi'' \approx 0.43$ for all values of grain radii and superconducting fractions. We can also observe 4 distinct changes in slope of $\chi'' vs T$ curve in the region of decreasing temperature from T_p to T_l.

4.4 Summary

Comparison between the 1D and 2D critical state model illustrates the similarity of qualitative global results in both Rademacher and Repetitive Gaussian pinned samples. Major trends in χ'' peak position vs T variations with grain radii and pinning strength remains the same and independent of dimensionality of the sam-

ple. T_p decreases with increase in grain radii. Even the value of χ'' peak changes only in the second decimal place between 1D and 2D model. However, the nature of χ'' vs T graph shows variation and more pronounced changes in slope. In RD pinned sample, abrupt changes are noticed which were absent in the one dimensional sample.

4.5 Future Direction of Research

- The effect of change in R/λ ratio has been modelled entirely by changing R. Given that London penetration depth in pnictides have a range of values, change in λ for a fixed value of R could be investigated.
- Effect of a mixed ac + dc magnetic field on the proposed model can be of interest.
- Different temperature dependence of penetration depth in low temperature region and near T_c would make the model more realistic.
- In the 2D case, different pinning strengths and/or different pinning functions could be an area of study.
- Explanations for kinks in χ'' vs T graph is being sought.

References

[1] D. Dew-Hughes, Phil. Mag. 30 (1974) 293.

[2] E. H. Brandt and M. Indenbom, Phys. Rev. B **48**, 12893(1993)

[3] K. H. Muller, Physica C **159**, (1989) 717

[4] C. Reichhardt and C. J. Olson Reichhardt, Phys. Rev. B **76**, 064523 (2007).

[5] T. H. Johansen and H. Bratsberg, J. Appl. Phys. **77**, 3945(1995)

[6] C.Romero-Salazar and F.Pérez-Rodŕiguez, Appl. Phys. Lett. **83**, 5256(2003)

[7] H. Dersch and G. Blatter, Phys. Rev. B **38**, 11391 (1988)

[8] M. Däumling and D. C. Larbalestier, Phys. Rev. B **40**, 9350(R)(1989)

[9] L. W. Conner and A. P. Malozemoff, Phys. Rev. B **43**, 402(1991)

[10] J. R. Clem, Phys. Rev. B **43**, 7837(1991)

[11] J. R. Clem and A. Sanchez, Phys. Rev. B **50**, 9355(1994)

[12] S. Roy and A. K. Ghosh, Physica C **580**, 1353766(2021)

Appendix I

Code in C for Repetitive Gaussian Sample

I.1 Single Temperature Field Profile

Code for field profile generation in a Repetitive Gaussian pinned sample is shown at a single temperature $T = 35$. Gaussian pinning constant $\alpha_G = 6.0\text{x}10^5$. Variable for temperature loop *ntemp* is defined as 1 and the temperature loop (line 89 in the program) runs only once. For complex susceptibility calculation, this loop is run over the entire temperature range 1 to 51.

```
1 #include <stdio.h>
2 #include <math.h>
3 #include <stdlib.h>
4
5 double* rk4solver(double x2, int x3);
6 double derivative( double y1, double y2, int y3);
7 float bessi0(float x1);
8 float bessi1(float x2);
```

```
9
10 #define d 1.0
11 #define nogs 215
12 #define R (0.00004*2)
13 #define noseg 5
14 #define seglength (d/noseg)
15 #define fs ((nogs*2.0*R*noseg)/d)
16 #define fn (1-fs)
17 #define ngsegl ((fn*d)/noseg)
18 #define gsegl (seglength-ngsegl)
19 #define sigma (ngsegl/6)
20
21 #define ngendpoint1 (-d+ngsegl)
22 #define segmentend1 (-d+(d/noseg))
23 #define ngendpoint2 (segmentend1+ngsegl)
24 #define segmentend2 (segmentend1+seglength)
25 #define ngendpoint3 (segmentend2+ngsegl)
26 #define segmentend3 (segmentend2+seglength)
27 #define ngendpoint4 (segmentend3+ngsegl)
28 #define segmentend4 (segmentend3+seglength)
29 #define ngendpoint5 (segmentend4+ngsegl)
30 #define segmentend5 (segmentend4+seglength)
31
32 #define peakpos1 (-d+ngsegl/2)
33 #define peakpos2 (peakpos1+seglength)
```

```
34 #define peakpos3 (peakpos2+seglength)
35 #define peakpos4 (peakpos3+seglength)
36 #define peakpos5 (peakpos4+seglength)
37
38 #define Gendpt1 (-d+(ngsegl+gsegl/2))
39 #define Gendpt2 (Gendpt1+seglength)
40 #define Gendpt3 (Gendpt2+seglength)
41 #define Gendpt4 (Gendpt3+seglength)
42
43
44 #define n 500000
45 #define ntemp 1
46 #define h (d/n)
47 #define tm 20
48 #define pi 3.14159265359
49 #define omega 314.15
50 #define lambda0 0.0000125
51 #define Tc 51.0
52 #define alphag 6.0e5
53 #define Hmaext 200.0
54
55 int counter=1, count=0;
56 //position, external magnetic field, average of field over
     position and effective permeability arrays
57 double xP[n+1],Hma[tm+1],Bp[tm+1],mu[tm+1];
```

```
58
59 //variable to assign sign to derivative depending on increase or
      decrease from previous time
60 double sign;
61 int dum=0;
62 int cnxp=1;
63 //magnetic field array [position] [time]
64 double H[n+1][tm+1];
65 // intial field,
66 double Hini=0.0,sumg=0.0,sumng=0.0,countng=0.0, coung=0.0, sum1,
      sum2,mueff=0.0;
67 double T=0.0, time=0.0;
68 double chip[ntemp], chidp[ntemp];
69
70 int main()
71 {
72
73  double angle=0.0, xini=-d;
74
75 for (int ctime=0; ctime<=tm; ctime++)
76  {
77      time=(2.0*pi*ctime)/(omega*tm);
78       H[0][ctime]=Hmaext*cos(omega*time);
79          Hma[ctime]=Hmaext*cos(omega*time);
80  }
```

```
81  FILE *f1 = fopen("xposition.txt", "w");
82  for (int cposition=0; cposition<=n; cposition++)
83   {
84    xP[cposition]=(cposition*h)-1.0;
85    fprintf(f1,"%f\n",xP[cposition]);
86   }
87  fclose(f1);
88
89  for (int ctemp=0; ctemp<ntemp;ctemp++)
90  {
91      T=35.0; // Temperature
92   sum1=0.0;
93   sum2=0.0;
94
95      for (int ctime=0; ctime<=tm; ctime++)
96  {
97      Hini=Hma[ctime];
98      sign=1;
99      if (ctime>=1)
100      {
101      if (Hma[ctime]-Hma[ctime-1]<0) sign=-1;
102      }
103      printf("Hini %f\n",Hini);
104     double *arr=rk4solver(Hini, sign);
105     mu[ctemp]=mueff;
```

```
106     for (int cposition=1; cposition<=n; cposition++)
107       {
108         H[cposition][ctime]= arr[cposition-1];
109       }
110
111       free(arr);
112       int cmid=tm/2;
113  if(ctime==0)
114     {
115      for(int cposition=0;cposition<=n;cposition++)
116       {
117        if (H[cposition][0]<=0) {H[cposition][0]=0;}
118       }
119      }
120 else if(ctime<=cmid)
121   {
122      for (int cposition=0; cposition<=n;cposition++)
123      {
124          if (H[cposition][ctime]>H[cposition][ctime-1])
125              {
126                  int posindexdum=cposition;
127                   for (; posindexdum<=n;posindexdum++)
128                   {
129                         H[posindexdum][ctime]=H[posindexdum][0];
130                   }          break;
```

```
131                 }
132               }
133           }
134       else
135           {
136            for (int cposition=0; cposition<=n;cposition++)
137            {
138                 if (H[cposition][ctime]<H[cposition][ctime-1])
139                    {
140                        int posindexdum=cposition;
141                         for (; posindexdum<=n;posindexdum++)
142                         {
143                               H[posindexdum][ctime]=H[posindexdum][cmid];
144                         }          break;
145                    }
146            }
147           }
148
149
150           double xpdum=0.0;
151           double Hdum=0.0;
152           sumg=0.0; int countg=0;
153           sumng=0.0; int countng=0;
154          for(int cposition=0; cposition<=n; cposition++)
155           {
```

```
156         xpdum=xP[cposition];
157         Hdum=H[cposition][ctime];
158         if(xpdum<=ngendpoint1 || (xpdum>=segmentend1 && xpdum<=
    ngendpoint2 )||(xpdum>=segmentend2 && xpdum<=ngendpoint3) ||(
    xpdum>=segmentend3 && xpdum<=ngendpoint4) || (xpdum>=
    segmentend4 && xpdum<=ngendpoint5))
159           {
160            sumng=sumng+(Hdum*mueff);
161            countng=countng+1;
162           }
163         else
164           {
165                sumg=sumg+(Hdum*(1.0-mueff));
166              countg=countg+1;
167           }
168
169      }
170  Bp[ctime]=(sumng/countng)+(sumg/countg);
171 printf("%f \n", Bp[ctime]);
172
173  FILE *fHJ = fopen("HJ.txt", "w");
174  FILE *fxJ = fopen("xJ.txt", "w");
175  FILE *fHg = fopen("Hg.txt", "w");
176  FILE *fxg = fopen("xg.txt", "w");
177
```

```
178  for (int c=0; c<=n; c++)
179   {
180    xpdum=xP[c];
181   for (int cnt=0; cnt<=tm; cnt++)
182    {
183     Hdum=H[c][cnt];
184   if(xpdum<=ngendpoint1 || (xpdum>=segmentend1 && xpdum<=
      ngendpoint2 )||(xpdum>=segmentend2 && xpdum<=ngendpoint3) || (
      xpdum>=segmentend3 && xpdum<=ngendpoint4) || (xpdum>=
      segmentend4 && xpdum<=ngendpoint5))
185         {
186           fprintf(fHJ,"%f ",Hdum);
187          if(cnt==0){ fprintf(fxJ,"%f ",xpdum);}
188           if (cnt==tm)
189          {
190            fprintf(fHJ,"\n");
191            fprintf(fxJ,"\n");
192           }
193
194     }
195    else
196 {
197          fprintf(fHg,"%f ",Hdum);
198           if(cnt==0) { fprintf(fxg,"%f ",xpdum);}
199       if (cnt==tm)
```

```
200             {
201                 fprintf(fHg,"\n");
202                 fprintf(fxg,"\n");
203               }
204             }
205         }
206
207     }
208 fclose(fxJ);
209 fclose(fHJ);
210 fclose(fxg);
211 fclose(fHg);
212
213  time=(2.0*pi*ctime)/(omega*tm);
214     sum1+=(Bp[ctime]*cos(omega*time));
215     sum2+=(Bp[ctime]*sin(omega*time));
216 }
217
218    chip[ctemp]=-1.0+2.0*(sum1/(Hmaext*(tm+1.0)));
219    chidp[ctemp]=2.0*(sum2/(Hmaext*(tm+1.0)));
220    printf(" %f, %f, %f \n\n ", T, chip[ctemp], chidp[ctemp]);
221    FILE *fmu = fopen("chi.txt", "a");
222       fprintf(fmu,"%f %f %f\n",T,chip[ctemp],chidp[ctemp]);
223       fclose(fmu);
224       printf("%d\n",ctemp);
```

```
225  }
226
227  return 0;
228 }
229
230 double* rk4solver(double h2,int s1)
231 {
232
233    printf("Hini %f\n",h2);
234     double k1,k2,k3,k4,lambda, ratio;
235      double xpos=0.0;
236     lambda= lambda0+pow((T/Tc),2.0);
237     ratio=R/lambda;
238     mueff=fn+ fs*((2.0* bessi1(ratio))/(ratio*bessi0(ratio)));
239
240     double *H2= (double*)malloc(sizeof(double)*n);
241      dum+=1;
242
243     for (int c=0; c<n; c++)
244     {
245          xpos=xP[c];
246          k1=h*derivative(xpos,h2,s1);
247          k2=h*derivative(xpos+h/2.0, h2+k1/2.0,s1);
248          k3=h*derivative(xpos+h/2.0, h2+k2/2.0,s1);
249          k4=h*derivative(xpos+h, h2+k3,s1);
```

```
250         *(H2+c)=h2+k1/6.0+k2/3.0+k3/3.0+k4/6.0;
251         h2=*(H2+c);
252
253     }
254      counter+=1;
255       return H2;
256       }
257
258     double derivative(double x3, double h3, int s3)
259 {
260     double dhdx, expval,h3p, Tval,MU;
261
262     Tval=pow((1.0-(T/Tc)),2.0);
263
264     if (x3<=Gendpt1) expval =exp(-pow(x3-peakpos1,2)/(2*pow(sigma
    ,2.0)));
265     else if (x3<=Gendpt2) expval =exp(-pow(x3-peakpos2,2)/(2*pow(
    sigma,2.0)));
266     else if (x3<=Gendpt3) expval =exp(-pow(x3-peakpos3,2)/(2*pow(
    sigma,2.0)));
267     else if (x3<=Gendpt4) expval =exp(-pow(x3-peakpos4,2)/(2*pow(
    sigma,2.0)));
268     else expval =exp(-pow(x3-peakpos5,2)/(2*pow(sigma,2.0)));
269
```

```
270 if(x3<=ngendpoint1 || (x3>=segmentend1 && x3<=ngendpoint2 ) || (
    x3>=segmentend2 && x3<=ngendpoint3) ||( x3>=segmentend3 && x3
    <=ngendpoint4) || (x3>=segmentend4 && x3<=ngendpoint5))
271         {
272          MU=mueff;
273         }
274        else
275         {
276              MU=1.0;
277         }
278
279      dhdx= -s3*((alphag*expval*Tval)/(MU*(fabs(h3)+0.1)));
280
281
282       if (dum==1 && cnxp%4==1)
283      {
284      FILE *f = fopen("alphasubJ0supGofx.txt", "a");
285      fprintf(f," %f\n", alphag*expval);
286      fclose(f);
287      }
288      cnxp+=1;
289      return dhdx;
290
291 }
292
```

```
293 float bessi0(float x1)
294 //Returns the modified Bessel function I0(x) for any real x.
295 {
296 float ax,ans;
297 double y; //Accumulate polynomials in double precision.
298 if ((ax=fabs(x1)) < 3.75) { //Polynomial fit.
299 y=x1/3.75;
300 y*=y;
301 ans=1.0+y*(3.5156229+y*(3.0899424+y*(1.2067492
302 +y*(0.2659732+y*(0.360768e-1+y*0.45813e-2)))));
303 } else {
304 y=3.75/ax;
305 ans=(exp(ax)/sqrt(ax))*(0.39894228+y*(0.1328592e-1
306 +y*(0.225319e-2+y*(-0.157565e-2+y*(0.916281e-2
307 +y*(-0.2057706e-1+y*(0.2635537e-1+y*(-0.1647633e-1
308 +y*0.392377e-2)))))));
309 }
310 return ans;
311 }
312 //#include <math.h>
313 float bessi1(float x2)
314 //Returns the modified Bessel function I1(x) for any real x.
315 {
316 float ax,ans;
317 double y;// Accumulate polynomials in double precision.
```

```
318 if ((ax=fabs(x2)) < 3.75) {// Polynomial fit.
319 y=x2/3.75;
320 y*=y;
321 ans=ax*(0.5+y*(0.87890594+y*(0.51498869+y*(0.15084934
322 +y*(0.2658733e-1+y*(0.301532e-2+y*0.32411e-3))))));
323 } else {
324 y=3.75/ax;
325 ans=0.2282967e-1+y*(-0.2895312e-1+y*(0.1787654e-1
326 -y*0.420059e-2));
327 ans=0.39894228+y*(-0.3988024e-1+y*(-0.362018e-2
328 +y*(0.163801e-2+y*(-0.1031555e-1+y*ans))));
329 ans *= (exp(ax)/sqrt(ax));
330 }
331 return x2 < 0.0 ? -ans : ans;
332 }
```

For the Rademacher pinned sample, only the function called derivative is different.

```
1 double derivative(double x3, double h3, int s3)
2 {
3     double dhdx, stepval,h3p, Tval, MU;
4     Tval=pow((1.0-(T/Tc)),2.0);
5
6 if(x3<=ngendpoint1 || (x3>=segmentend1 && x3<=ngendpoint2 ) || (
   x3>=segmentend2 && x3<=ngendpoint3) ||( x3>=segmentend3 && x3
```

```
   <=ngendpoint4) || (x3>=segmentend4 && x3<=ngendpoint5))
7          {
8           MU=mueff;
9            stepval =1.0;
10         }
11        else
12         {
13             MU=1.0;
14           stepval =0.0;
15         }
16
17
18       dhdx= -s3*((alphas*stepval*Tval)/(MU*(fabs(h3)+0.1)));
19       if (dum==1 && cnxp%4==1)
20       {
21      FILE *f = fopen("alphasubJ0supRDofx.txt", "a");
22       fprintf(f," %f\n", alphas*stepval);
23       fclose(f);
24
25       }
26        cnxp+=1;
27
28       return dhdx;
29  }
```

Appendix II

Changes in code for 2D pinned sample

Both x-component and y-component of the total field are calculated with different RK4 solver functions with separate calls to a derivative function as defined in Appendix I, which computes magnetic field with position inside the sample in accordance with the current-field relationship and returns the value as an array. The reason for doing this is that the identical components along different axes is just the starting point of the 2D scenario and having separate solvers makes it easier to program different pinning defects, different pinning density profile along different axes.

After we call the RK4 solvers in the main function, we compute total field at each point while accounting for its position being either in the grained or grain-free region in the sample. This also affects the effective permeability and that has to be taken into account separately.